

## Renormalisation running of masses and mixings in UED models

A.S. Cornell

*National Institute for Theoretical Physics; School of Physics,  
University of the Witwatersrand, Wits 2050, South Africa  
alan.cornell@wits.ac.za*

Aldo Deandrea

*Université de Lyon, F-69622 Lyon, France;  
Université Lyon 1, CNRS/IN2P3, UMR5822 IPNL, F-69622 Villeurbanne Cedex, France  
deandrea@ipnl.in2p3.fr*

Lu-Xin Liu

*National Institute for Theoretical Physics; School of Physics,  
University of the Witwatersrand, Wits 2050, South Africa  
luxin.liu9@gmail.com*

Ahmad Tarhini

*Université de Lyon, F-69622 Lyon, France;  
Université Lyon 1, CNRS/IN2P3, UMR5822 IPNL, F-69622 Villeurbanne Cedex, France  
tarhini@ipnl.in2p3.fr*

We review the Universal Extra-Dimensional Model compactified on a  $S^1/Z_2$  orbifold, and the renormalisation group evolution of quark and lepton masses, mixing angles and phases both in the UED extension of the Standard Model and of the Minimal Supersymmetric Standard Model. We consider two typical scenarios: all matter fields propagating in the bulk, and matter fields constrained to the brane. The resulting renormalisation group evolution equations in these scenarios are compared with the existing results in the literature, together with their implications.

*Keywords:* Beyond the Standard Model; Extra Dimensional Model; Renormalisation Group Equations; Supersymmetry; CKM Matrix; PMNS Matrix.

11.10.Hi, 11.10.Kk, 12.60.Jv, 14.60.Pq, 12.15.Ff

### 1. Introduction

The Standard Model (SM), by meeting all confrontations with experiments, stands as a remarkably simple parameterisation of known physics. Yet it has many unsatisfactory aspects such as a large number of parameters, a triplication of chiral families, and three different gauge structures. Consequently, it is strongly believed among theorists that there must exist a simpler underlying structure of which the SM is the low energy piece. Many think that such a structure will make its appear-

ance at much higher energies, somewhere in the unexplored region between a few TeV and the Planck scale. Experimentalists can only proceed one or two orders of magnitude at a time in their exploration of those scales. Theorists, on the other hand, have mainly a twofold approach in divining this structure. In the first, the quantum numbers of the SM are grouped into mathematically pleasing structures (constrained however by the predictions affecting the low energy part of the theory), resulting in an exercise in quantum pattern recognition. This has led to Grand Unified Theories (GUTs) [1]. The second approach is to use the renormalisation group to extrapolate the SM parameters to the unexplored scales [2]. The purpose is to find if those parameters satisfy interesting relations at higher energies. When used in conjunction with the former approach, this can give powerful hints of the physics expected at higher energies.

We shall also recall that in order to obtain finite results in quantum field theory, in a higher order than the tree level, one has to perform the renormalisation program. The independence of the renormalisation procedure from the renormalisation point leads to the dependence of the Lagrangian parameters on the point of renormalisation. This dependence is governed by the Renormalisation Group Equations (RGEs) for the coupling constants and other parameters of the Lagrangian. As such, it all depends on having accurate data to input as initial conditions on the RGEs, as well as a strong theoretical basis for the evolution equations themselves. These theories, at asymptotic energies, may reveal some new symmetries or other interesting properties that give deeper insight into the physical content. Also, from the requirement of the stability of the theory one can, for example, give bounds on the physical parameters, like the Higgs mass in the SM or its extensions.

In the SM, the runnings of the gauge, Yukawa and quartic scalar couplings is logarithmic with the energy scale. Although the gauge couplings do not all meet at a point, they tend to unify near  $10^{15}$  GeV. Extensions to the SM such as extra-dimensional scenarios accessible to SM fields have the virtue, thanks to the couplings now having a power law running, of bringing the unification scale down to an explorable range [3]. Note that many other extensions to the SM exist which alter the runnings in different ways, such as supersymmetry, where a range of new particles ensure the gauge couplings do meet at a point, but runnings remain logarithmic. However, combinations of the different approaches have led, in the last two decades, to some extremely interesting phenomenological models, such as TeV scale extra-dimensional scenarios giving rise to new supersymmetry breaking mechanisms [4], as well as addressing fermion mass hierarchy [5] and providing cosmologically viable dark matter candidates [6].

With the Large Hadron Collider (LHC) now up and running, exploration of the realm of new physics that may operate at the TeV scale has begun. Among these models those with extra spatial dimensions might be revealed in such higher energy collider experiments, where the Universal Extra Dimension (UED) model makes for an interesting TeV scale physics scenario; as it features a tower of Kaluza-Klein (KK) states for each of the SM fields, all of which have full access to the extended space-

time manifold [7]. This particular scenario has recently been extensively studied in the literature, such as investigations of electroweak symmetry breaking, proton stability, gauge hierarchy and fermion mass hierarchy problems,  $B$  physics, dark matter etc. [8–13]. This model has been a fruitful playground for addressing a variety of puzzles in the SM.

We therefore collect in a comprehensive manner and in one place the necessary tools for making renormalisation group analyses of the SM and its UED extensions. We view this compendium as a template for general applications of the running of parameters from the  $m_Z$  scale to the Planck scale. The observable parameters of the SM are: 6 quark masses, 3 lepton masses, 4 parameters of the Cabibbo-Kobayashi-Maskawa (CKM) matrix [14] and 3 gauge couplings. The RGEs for the CKM matrix being obtained from the RGEs for the Yukawa couplings. This can also be extended to include neutrino masses and mixings possible in the leptonic sector, as we shall discuss further in section 9.

In this review we first introduce the various models and their varieties we shall consider (section 2 and section 3 for the supersymmetric extensions to this), next deriving the RGEs for the gauge couplings constants (section 4) and Yukawa couplings for the SM and UED scenarios (section 5) and 5-dimensional Minimal Supersymmetric SMs (5D MSSM) (section 6). This shall be followed by a review of the CKM parameters evolution (sections 7 and 8). Extensions to massive neutrino scenarios and their mixings evolution will follow in section 9. With a summary and our conclusions in section 10.

## 2. The UED Standard Model

The UED model places particles of the SM in the bulk of one or more compactified extra dimensions. In our case we have a single flat extra dimension of size  $R$ , compactified on an  $S_1/Z_2$  orbifold. As such we will have an infinite tower of KK modes with the zero modes corresponding to the SM states. These KK modes are in the TeV scale and modify the running of the RGEs at relatively low energy scales. The UED model, like any higher dimensional theory, is an effective field theory which is valid up to some scale  $\Lambda$ , at which a new physics theory emerges. Between the scale  $R^{-1}$  where the first KK states are excited and the cutoff scale  $\Lambda$ , there are finite quantum corrections to the Yukawa and gauge couplings from the  $\Lambda R$  number of KK states. Up to the scale  $R^{-1}$  the first step KK excitation occurs, the RG evolution is logarithmic, controlled by the SM beta functions. With the increasing of the energy, that is, when the KK threshold is crossed for each successive mode, new excitations come into play and govern new sets of beta functions. The values of physical parameters such as Yukawa couplings and gauge couplings do not run in the old SM fashion, instead they receive finite quantum corrections whose magnitudes depend explicitly on the value of this cutoff parameter. As a result, once the KK states are excited, these couplings exhibit power law dependencies on  $\Lambda$ . This can be illustrated if  $\Lambda R \gg 1$ , to a very good accuracy, the generic SM beta function

is shown to have the power law evolution behaviour [10]:

$$\beta^{4D} \rightarrow \beta^{4D} + (S(\mu) - 1) \tilde{\beta}, \quad (1)$$

where  $\tilde{\beta}$  is a generic contribution from a single KK level, and where its coefficient is not a constant but instead  $S(\mu) = \mu R$ , with  $\mu^{Max} = \Lambda$ , reflecting the power law running behaviour. As a result of faster running, the gauge couplings tend to lower the unification scale down to a relatively low order, which might be accessible to collider experiments, such as the LHC or the proposed International Linear Collider (ILC). Therefore, constraints from precision electroweak tests and current (or future) collider data would yield bounds on the compactification radius  $R$ . The RGE are an important tool for the search of the properties of the quark masses and the Cabibbo-Kobayashi-Maskawa (CKM) matrix at different energy scales. It is therefore of great interest to have an implementation of the UED model in studying these RGE.

The first version of this model we shall consider, the bulk UED model, sometimes known as the minimal UED model, has one extra dimension compactified on a circle of radius  $R$  with a  $Z_2$  orbifolding which identifies the fifth coordinate  $y \rightarrow -y$ . The 5-dimensional KK expansions of the weak doublet and singlet as well as the Higgs and gauge fields are shown (the corresponding coupling constants among the KK modes are simply equal to the SM couplings up to normalisation factors, e.g.  $Y_U = \frac{Y_U^5}{\sqrt{\pi R}}$ ) below:

$$\begin{aligned} H(x, y) &= \frac{1}{\sqrt{\pi R}} \left\{ H(x) + \sqrt{2} \sum_{n=1}^{\infty} H_n(x) \cos\left(\frac{ny}{R}\right) \right\}, \\ A_\mu(x, y) &= \frac{1}{\sqrt{\pi R}} \left\{ A_\mu^0(x) + \sqrt{2} \sum_{n=1}^{\infty} A_\mu^n(x) \cos\left(\frac{ny}{R}\right) \right\}, \\ u(x, y) &= \frac{1}{\sqrt{\pi R}} \left\{ u_R(x) + \sqrt{2} \sum_{n=1}^{\infty} \left[ u_R^n(x) \cos\left(\frac{ny}{R}\right) + u_L^n(x) \sin\left(\frac{ny}{R}\right) \right] \right\}, \\ Q(x, y) &= \frac{1}{\sqrt{\pi R}} \left\{ q_L(x) + \sqrt{2} \sum_{n=1}^{\infty} \left[ Q_L^n(x) \cos\left(\frac{ny}{R}\right) + Q_R^n(x) \sin\left(\frac{ny}{R}\right) \right] \right\}, \\ d(x, y) &= \frac{1}{\sqrt{\pi R}} \left\{ d_R(x) + \sqrt{2} \sum_{n=1}^{\infty} \left[ d_R^n(x) \cos\left(\frac{ny}{R}\right) + d_L^n(x) \sin\left(\frac{ny}{R}\right) \right] \right\}, \\ L(x, y) &= \frac{1}{\sqrt{\pi R}} \left\{ L_L(x) + \sqrt{2} \sum_{n=1}^{\infty} \left[ L_L^n(x) \cos\left(\frac{ny}{R}\right) + L_R^n(x) \sin\left(\frac{ny}{R}\right) \right] \right\}, \\ e(x, y) &= \frac{1}{\sqrt{\pi R}} \left\{ e_R(x) + \sqrt{2} \sum_{n=1}^{\infty} \left[ e_R^n(x) \cos\left(\frac{ny}{R}\right) + e_L^n(x) \sin\left(\frac{ny}{R}\right) \right] \right\}. \quad (2) \end{aligned}$$

The zero modes in the above equations are identified with the 4-dimensional SM fields, whilst the complex scalar field  $H$  and the gauge field  $A_\mu$  are  $Z_2$  even fields,

and there is a left-handed and a right-handed KK mode for each SM chiral fermion. Note that in models with UED momentum conservation in the extra dimensions, we are led to the conservation of KK number at each vertex in the interactions of the 4-dimensional effective theory (or strictly speaking, the KK parity  $(-1)^n$  is what remains conserved, where  $n$  is the KK number). In the bulk we have the fermion and gauge field interactions as follows:

$$\begin{aligned}\mathcal{L}_{Leptons} &= \int_0^{\pi R} dy \{ i\bar{L}(x, y) \Gamma^M \mathcal{D}_M L(x, y) + i\bar{e}(x, y) \Gamma^M \mathcal{D}_M e(x, y) \} , \\ \mathcal{L}_{Quarks} &= \int_0^{\pi R} dy \{ i\bar{Q}(x, y) \Gamma^M \mathcal{D}_M Q(x, y) + i\bar{u}(x, y) \Gamma^M \mathcal{D}_M u(x, y) + i\bar{d}(x, y) \Gamma^M \mathcal{D}_M d(x, y) \} ,\end{aligned}\tag{3}$$

where  $\Gamma^M = (\gamma^\mu, i\gamma^5)$ , and  $M = 0, 1, 2, 3, 5$ . Explicitly, the kinetic terms are given by:

$$\begin{aligned}\mathcal{D}_M Q(x, y) &= \left( \partial_M + ig_3^5 G_M + ig_2^5 W_M + i\frac{1}{6}g_1^5 B_M \right) Q(x, y) , \\ \mathcal{D}_M u(x, y) &= \left( \partial_M + ig_3^5 G_M + i\frac{2}{3}g_1^5 B_M \right) u(x, y) , \\ \mathcal{D}_M d(x, y) &= \left( \partial_M + ig_3^5 G_M + i\frac{-1}{3}g_1^5 B_M \right) d(x, y) , \\ \mathcal{D}_M L(x, y) &= \left( \partial_M + ig_2^5 W_M + i\frac{-1}{2}g_1^5 B_M \right) L(x, y) , \\ \mathcal{D}_M e(x, y) &= (\partial_M - ig_1^5 B_M) e(x, y) .\end{aligned}\tag{4}$$

The gauge couplings  $g_3^5$ ,  $g_2^5$  and  $g_1^5$  refer to those of the  $SU(3)$ ,  $SU(2)$  and  $U(1)$  gauge groups respectively, and are related to the 4-dimensional SM coupling constants by  $g_i = \frac{g_i^5}{\sqrt{\pi R}}$ , and the five dimensional gauge fields have the generic form  $A_M = (A_\mu, A_5)$ . After integrating out the compactified dimension, the 4-dimensional effective Lagrangian has interactions involving the zero mode and the KK modes. However, these KK modes cannot affect electroweak processes at tree level, and only contribute to higher order electroweak processes. For the one-loop diagrams of the Yukawa couplings we choose the Landau gauge in what follows, as many one-loop diagrams are finite in the Landau gauge and have no contribution to the renormalisation of the Yukawa couplings. We therefore consider the RGE for the quark- Higgs Yukawa couplings from which we obtain the evolution of the quark masses and the CKM matrix. The one-loop Feynman diagram contributions to the Yukawa couplings in the SM and UED model have been explicitly illustrated in [10, 15–17]. In the UED model, where for each energy level  $n_i$ , we effectively have a heavier duplicate copy of the entire SM particle content. That is, at each KK

excited level, the KK tower corresponding to the fields in Eq. (2) exactly mirror the SM field ground states. However, new contributions from the  $A_5$ ,

$$A_5(x, y) = \sqrt{\frac{2}{\pi R}} \sum_{n=1}^{\infty} A_5^n(x) \sin\left(\frac{ny}{R}\right), \quad (5)$$

interactions (that of the fifth component of the vector fields, i.e.  $A_5 = \{G_5, W_5, B_5\}$ ) also contribute. In contrast, the fifth component of the gauge bosons  $A_5(x, y)$  is a real scalar and does not have any zero mode, transforming in the adjoint representation of the gauge group.

A simple alternative to this model is that of the brane localised UED model, where we have the same fields but where the fermion matter fields cannot propagate in the bulk and they are restricted to the brane. In the brane localised UED model, extra dimensional models make an interesting TeV scale physics scenario and as discussed earlier might be revealed in higher energy collider experiments, as they feature states that have full access to the extended space-time manifold. For the case of brane localised matter fields, only the boson fields (the gauge fields and the scalar fields) can propagate in the bulk space. However, if the compactification radius  $R$  is sufficiently large, due to the power law running of the gauge couplings, it will enable us to bring the unification scale down to an exportable range at the LHC scale.

### 3. The 5D MSSM

Another useful model we shall consider is the 5D MSSM defined in [3, 18–26]. The 5D MSSM is a five dimensional  $\mathcal{N} = 1$  supersymmetric model compactified on the  $S_1/Z_2$  orbifold which breaks the 5D Lorentz invariance to the usual 4D one. This breaking gives a momentum conservation along the fifth dimension which conserves the KK number at tree level and KK parity at loop level. One of the main implications of KK-parity invariance is that the lightest KK mode is stable and can be a cold dark matter candidate. In this compactification we can recover the MSSM at zero mode since we obtain chiral fermions. Note though, that since we are working with a supersymmetric model, the beta function can be derived in the superfield formalism, where we shall discuss  $\mathcal{N} = 1$  supersymmetry in a five-dimensional Minkowski space and its description in terms of 4D superfields. The space-time coordinates being labelled by  $(x^\mu, y)$ .

The gauge sector is then described by a 5D  $\mathcal{N} = 1$  vector supermultiplet which consists (on-shell) of a 5D vector field  $A^M$ , a real scalar  $S$  and two gauginos,  $\lambda$  and  $\lambda'$ . The action for which can be given by:

$$S_g = \int d^5x \frac{1}{2kg^2} \text{Tr} \left[ -\frac{1}{2} F^{MN} F_{MN} - D^M S D_M S - i\bar{\lambda} \Gamma^M D_M \lambda - i\bar{\lambda}' \Gamma^M D_M \lambda' + (\bar{\lambda} + \bar{\lambda}') [S, \lambda + \lambda'] \right], \quad (6)$$

with  $D_M = \partial_M + iA_M$  and  $\Gamma^M = (\gamma^\mu, i\gamma^5)$ .  $F^{MN} = -\frac{i}{g}[D^M, D^N]$  and  $k$  normalises the trace over the generators of the gauge groups.

From the decomposition of the 5D supercharge (which is a Dirac spinor) into two Majorana-type supercharges, which constitute a  $\mathcal{N} = 2$  superalgebra in 4D, one can rearrange these fields in terms of a  $\mathcal{N} = 2$ , 4D vector supermultiplet,  $\Omega = (V, \chi)$ :

- $V$  :  $\mathcal{N} = 1$  vector supermultiplet containing  $A^\mu$  and  $\lambda$ ,
- $\chi$  :  $\mathcal{N} = 1$  chiral supermultiplet containing  $\lambda'$  and  $S' = S + iA^5$ .

Both  $V$  and  $\chi$  (and their component fields) are in the adjoint representation of the gauge group  $\mathcal{G}$ . Using the supermultiplets one can write the original 5D  $\mathcal{N} = 1$  supersymmetric action Eq.(6) in terms of  $\mathcal{N} = 1$  4D superfields and the covariant derivative in the  $y$  direction [21]:

$$S_g = \int d^5x d^2\theta d^2\bar{\theta} \frac{1}{4kg^2} \text{Tr} \left[ \frac{1}{4} (W^\alpha W_\alpha \delta(\bar{\theta}^2) + h.c) + (e^{-2gV} \nabla_y e^{2gV})^2 \right], \quad (7)$$

with  $W^\alpha = -\frac{1}{4}\bar{D}^2 e^{-2gV} D_\alpha e^{2gV}$ .  $D_\alpha$  is the covariant derivative in the 4D  $\mathcal{N} = 1$  superspace (see Refs [27,28].) and  $\nabla_y = \partial_y + \chi$ . To find the Feynman rules to a given order in the gauge coupling  $g$ , one can expand and quantise the action [18]. The beta functions for the couplings of the operators in the superpotential are governed by the wave function renormalisation constants  $Z_{ij} = 1 + \delta Z_{ij}$  due to the non-renormalisation theorem [29]. The Feynman diagrams related to the wave-function renormalisation are given in Fig.1.

The Higgs superfields and gauge superfields will always propagate into the fifth dimension. Different possibilities for the matter superfields will be discussed, where superfields containing SM fermions can propagate in the bulk or are restricted to

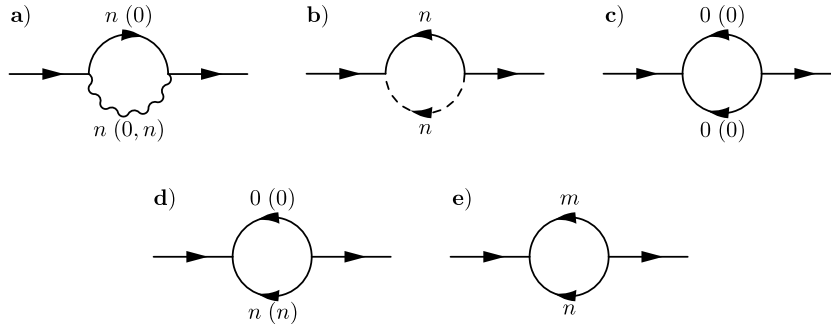


Fig. 1. The one-loop diagrams related to the wave-function renormalisation of the matter superfields, in which diagrams a)-e) refer to the case where all the matter fields are in the bulk, and the excited KK states are labelled by the number without the bracket; whereas diagrams a), c) and d) are related to the brane localised matter fields case, in which the KK states are labelled by the number inside the bracket [18, 23].

the brane. For the case where all fields can propagate in the bulk, the action for the matter fields would be [18]:

$$S_{matter} = \int d^8 z dy \left\{ \bar{\Phi}_i \Phi_i + \Phi_i^c \bar{\Phi}_i^c + \Phi_i^c \partial_5 \Phi_i \delta(\bar{\theta}) - \bar{\Phi}_i \partial_5 \bar{\Phi}_i^c \delta(\theta) \right. \\ \left. + \tilde{g}(2\bar{\Phi}_i V \Phi_i - 2\Phi_i^c V \bar{\Phi}_i^c + \Phi_i^c \chi \Phi_i \delta(\bar{\theta}) + \bar{\Phi}_i \bar{\chi} \bar{\Phi}_i^c \delta(\theta)) \right\} . \quad (8)$$

Again, this action can be expanded and quantised. The  $\chi$ -field should be odd under  $Z_2$  symmetry because it appears together with a derivative  $\partial_y$ , whereas  $V$  is even. For the two matter superfields, we choose  $\Phi$  to be even and the conjugate  $\Phi^c$  to be odd such that  $\Phi^c$  vanishes on the brane. Only the even fields have zero modes. The Fourier decomposition of the fields being:

$$V(x, y) = \frac{1}{\sqrt{\pi R}} \left[ V^{(0)}(x) + \sqrt{2} \sum_{n \geq 1} V^{(n)}(x) \cos\left(\frac{ny}{R}\right) \right] , \\ \chi(x, y) = \sqrt{\frac{2}{\pi R}} \sum_{n \geq 1} \chi^{(n)}(x) \sin\left(\frac{ny}{R}\right) , \quad (9) \\ \Phi(x, y) = \frac{1}{\sqrt{\pi R}} \left[ \Phi^{(0)}(x) + \sqrt{2} \sum_{n \geq 1} \Phi^{(n)}(x) \cos\left(\frac{ny}{R}\right) \right] , \\ \Phi^c(x, y) = \sqrt{\frac{2}{\pi R}} \sum_{n \geq 1} \Phi^{c(n)}(x) \sin\left(\frac{ny}{R}\right) .$$

We can write the action for the second case where all superfields containing SM fermions are restricted to the brane. In which case the part of the action involving only gauge and Higgs fields is not modified, whereas the action for the superfields containing the SM fermions becomes:

$$S_{matter} = \int d^8 z dy \delta(y) \left\{ \bar{\Phi}_i \Phi_i + 2\tilde{g} \bar{\Phi}_i V \Phi_i \right\} . \quad (10)$$

Due to the 5D  $\mathcal{N} = 1$  supersymmetry, Yukawa couplings are forbidden in the bulk. However, they can be introduced on the branes, which are 4D subspaces with reduced supersymmetry. One can also add the effective neutrino mass operator (also called lepton number violating Weinberg operator), with dimensional coupling  $\tilde{k}_{ij}$  in which we are interested to show its evolution and therefore the Majorana mass term for neutrinos. We will write the following interaction terms, called brane interactions, containing Yukawa-type couplings:

$$S_{brane} = \int d^8 z dy \delta(y) \left\{ \left( \frac{1}{6} \tilde{\lambda}_{ijk} \Phi_i \Phi_j \Phi_k - \frac{\tilde{k}_{ij}}{4M} L_i H_u L_j H_u \right) \delta(\bar{\theta}) + \text{h.c.} \right\} , \quad (11)$$

where  $L$  and  $H^u$  are the lepton and up-type Higgs doublet chiral superfields respectively. This operator is used to study neutrino masses and mixings, where RGEs for this effective operator have been derived in the context of the four-dimensional SM [30] and MSSM [31] and shall be discussed further in section 9. An extension



to compactified extra-dimensions was considered in Ref [18]. , and we shall use a similar formalism in the next section.

From Fig.1 we obtain the wave function renormalisation of the matter superfields and then we calculate the beta function. If we exclude the effects of extra dimensions, one can obtain the beta function of the usual MSSM. The Figs. 1a)-e) refer to the case where matter superfields are able to propagate in the bulk (excited KK states are labelled by the number without brackets) and diagrams in Figs.1 a), c), d) represent the case of brane localised matter superfields (excited KK states are labelled by the number inside brackets).

#### 4. Gauge couplings

The evolution of the gauge couplings in four dimension at one loop are given by:

$$16\pi^2 \frac{dg_i}{dt} = b_i g_i^3, \quad (12)$$

where  $b_i^{SM} = (\frac{41}{10}, -\frac{19}{6}, -7)$  and  $b_i^{MSSM} = (\frac{33}{5}, 1, -3)$  [32], using a  $SU(5)$  normalisation. If we consider our 5D theory as effective up to a scale  $\Lambda$ , we have contributions from the KK modes which give a power law evolution to the gauge couplings since extra-dimensions cause their running to vary much more rapidly. Eq.(1) can be written in terms of the scale parameter  $t$ :

$$16\pi^2 \frac{dg_i}{dt} = [b_i + (S(t) - 1)\tilde{b}_i] g_i^3, \quad (13)$$

where  $\tilde{b}_i$  take the following form in the case of the model UED SM [15, 33]:

$$(\tilde{b}_1, \tilde{b}_2, \tilde{b}_3) = \left( \frac{1}{10}, -\frac{41}{6}, -\frac{21}{2} \right) + \frac{8}{3}\eta, \quad (14)$$

with  $\eta$  being the number of generations of matter fields in the bulk. Therefore, for all our matter fields propagating in the bulk (that is,  $\eta = 3$ ), we have for the UED SM bulk case:

$$\tilde{b}_i = \left( \frac{81}{10}, \frac{7}{6}, -\frac{5}{2} \right). \quad (15)$$

Similarly, for all our matter fields localised to the 3-brane (that is,  $\eta = 0$ ), we have for the UED SM brane case:

$$\tilde{b}_i = \left( \frac{1}{10}, -\frac{41}{6}, -\frac{21}{2} \right). \quad (16)$$

Next we consider the beta functions of the gauge couplings in the 5D MSSM. In fact, after compactification of the 5D MSSM, we have two 4D  $\mathcal{N} = 1$  chiral supermultiplets,  $\Phi$  and  $\Phi^c$ , where the zero modes of  $\Phi$  give us the normal matter fields and Higgs fields as well as their super partners, while  $\Phi^c$  is a new supermultiplet. In the component field formalism, at each KK level, aside from the quantum corrections that mirror those of the 4D MSSM, the only new one-loop contributions to the  $A_\mu$  Feynman diagrams are from the wave function renormalisation of  $A_\mu$  (which

contribute via the coupling of  $A_\mu$  to the complex scalar field and its super-partner in the superfield  $\chi$ , and the coupling of  $A_\mu$  with the new fermion field and its super-partner in the superfield  $\Phi^c$  associated with the two doublets of the Higgs fields and the matter fields respectively in the bulk). This then gives rise to the master beta functions of the gauge couplings in the 5D MSSM as follows [23]:

$$(\tilde{b}_1, \tilde{b}_2, \tilde{b}_3) = \left(\frac{6}{5}, -2, -6\right) + 4\eta, \quad (17)$$

where  $\eta$  represents the number of generations of fermions which propagate in the bulk. So in the two cases we shall consider, that of all fields propagating in the bulk ( $\eta = 3$ ) we have [34]:

$$\tilde{b}_i = \left(\frac{66}{5}, 10, 6\right). \quad (18)$$

Similarly, for all our matter fields localised to the 3-brane (that is,  $\eta = 0$ ), we have:

$$\tilde{b}_i = \left(\frac{6}{5}, -2, -6\right). \quad (19)$$

In Figs.2 and 3 we have plotted the running of the gauge couplings for the UED SM case and the 5D MSSM respectively for the brane localised and bulk field cases, and for several choices of compactification scales for the extra- dimension ( $R$ ). From these plots, and the discussion given in Ref [34]. , we find that for the three gauge coupling constants to approach a small region at some value of  $t$  requires an extremely large value of  $1/R$ , which is of no phenomenological interest at present. For the case of our fields being brane localised in the UED model, we see a similar behaviour: the extra-dimensions naturally lead to gauge coupling unification at an intermediate mass scale for the compactification radii considered here. Furthermore, as illustrated in Fig.2, the extra space-time dimensions naturally lead to the appearance of GUTs at scales substantially below the usual GUT scale.

We assume the fundamental scale is not far from the range of LHC scale, and set the compactification radii to be  $R^{-1} = 2$  TeV, 8 TeV, and 15 TeV respectively. In the limit when the energy scale is much smaller than  $R^{-1}$ , since the energy of the system is less than the excitations of the first KK modes, the theory reduces to the usual 4-dimensional SM, and the existence of the KK excitations are ignored. When  $\mu > R^{-1}$ , excitations of many KK modes become possible, and the contributions of these KK states must be included in all physical calculations. This is characterised by the second term in Eq.(1) in the general beta function. Once the energy passes  $R^{-1}$  the excited KK modes tend to increase rapidly the running of the gauge couplings, and ultimately change the scale dependence of the gauge couplings from logarithmic to those of a power law as a function of  $\mu$ . Quantitatively, due to the fast running of the gauge couplings, we find they nearly meet at around  $t = 6.4, 7.8, 8.4$  for radii  $R^{-1} = 2, 8, 15$  TeV respectively. The extra dimensions naturally lead to gauge coupling unification at an intermediate mass scale.

Similarly, in Fig.3 we have plotted the evolutions of the brane localised and bulk field cases for several choices of compactification scales for the 5D MSSM. From these plots, and as noted above, we find that for the three gauge coupling constants to approach a small region at some value  $t$  requires an extremely large value of  $1/R$ , whereas, for the case of our fields being brane localised, the extra dimensions naturally lead to gauge coupling unification at a similarly valued intermediate mass scale for the compactification radii considered here.

### 5. Yukawa evolutions in the SM and UED SM

In the quark sector of the SM, we have ten experimentally measurable parameters, i.e. six quark masses, three mixing angles, and one phase (these angles and phase being encoded in the CKM matrix which we shall discuss in section 7). A completely satisfactory theory of fermion masses and the related problem of mixing

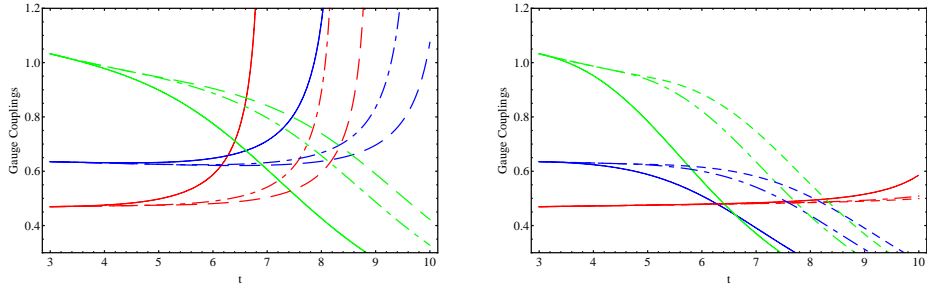


Fig. 2. Gauge couplings ( $g_1$  (red),  $g_2$  (blue),  $g_3$  (green)) with: in the left panel, all matter fields in the bulk (UED bulk); and the right panel for all matter fields on the brane (UED brane); for three different values of the compactification scales (2 TeV (solid line), 8 TeV (dot-dashed line), 15 TeV (dashed line)) as a function of the scale parameter  $t$  in the UED SM.

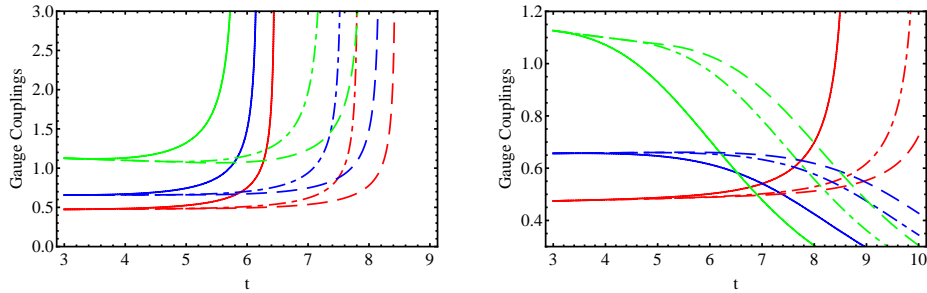


Fig. 3. Gauge couplings ( $g_1$  (red),  $g_2$  (blue),  $g_3$  (green)) with: in the left panel, all matter fields in the bulk; and the right panel for all matter fields on the brane; for three different values of the compactification scales (2 TeV (solid line), 8 TeV (dot-dashed line), 15 TeV (dashed line)) as a function of the scale parameter  $t$  in the 5D MSSM.

angles is certainly lacking at present, however, there has been considerable effort to understand the hierarchies of these mixing angles and fermion masses in terms of the RGEs [17, 32, 35–39]. First though we must recall that in order to explore the physics at a high energy scale we use RGEs as a probe to study the momentum dependence of the Yukawa couplings, the gauge couplings, and from these the CKM matrix elements themselves. As such we can consider one of the primary goals of the LHC as being to uncover any new dynamics within the TeV range, where instead of assuming the RGE goes from the  $M_Z$  scale up to the GUT scale ( $10^{15}$  GeV) by using the  $SU_C(3) \times SU_L(2) \times U_Y(1)$  symmetry, we know that models with extra dimensions may bring down the unification to a much lower energy scale. However, when using the RGEs as a probe, the initial values we shall adopt are very important, where we shall scale for the gauge couplings and the fermion masses at the  $M_Z$  scale are shown in Table 1.

Table 1. Initial values for the gauge couplings, fermion masses and CKM parameters at  $M_Z$  scale. Data is taken from Ref [23, 40, 41]..

Parameter	Value	Parameter	Value
$\alpha_1$	0.01696	$m_e$	0.48657 MeV
$\alpha_2$	0.03377	$m_\mu$	102.718 MeV
$\alpha_3$	0.1184	$m_\tau$	1746.24 MeV
$m_u$	1.27 MeV	$ V_{ub} $	0.00347
$m_c$	0.619 GeV	$ V_{cb} $	0.0410
$m_t$	171.7 GeV	$ V_{us} $	0.2253
$m_d$	2.90 MeV	$J$	$2.91 \times 10^{-5}$
$m_s$	55 MeV		
$m_b$	2.89 GeV		

Furthermore, we shall also attempt, in section 9, to develop the RGEs of the lepton sector (including possible mixing angles and phases), which will require knowledge of the evolution of a parameter  $k$ , where the lowest order operator which generates Majorana neutrino masses after electroweak symmetry breaking (EWSB), is the lepton-number violating Weinberg operator [42]. This lowest order operator (appearing with dimension  $d = 5$  in four space-time dimensions) can be written as:

$$-\frac{\tilde{k}_{ij}}{4M}(\bar{L}_\alpha^{ci}\epsilon^{\alpha\beta}\phi_\beta)(L_\delta^j\epsilon^{\delta\gamma}\phi_\gamma) + h.c. , \quad (20)$$

where  $L$  and  $\phi$  are the lepton and the Higgs doublet fields.  $M$  is the typical heavy energy scale for the range of validity of the low-energy effective theory. An operator of this type can be generated, for instance, by the usual see-saw mechanism. In which case the heavy scale  $M$  can be identified with the mass of the heavy right-handed neutrino. After EWSB the Higgs acquires a vacuum expectation value (vev) and the operator in Eq. (20) gives a Majorana mass term for the neutrinos. In the

context of the MSSM it can be written in the form:

$$-\frac{\tilde{k}_{ij}}{4M}(L_\alpha^i \epsilon^{\alpha\beta} H_\beta^u)(L_\delta^j \epsilon^{\delta\gamma} H_\gamma^u), \quad (21)$$

where  $L$  and  $H^u$  are the lepton and up-type Higgs doublet chiral superfields respectively. This operator is crucial for the study of neutrino masses and mixings, where renormalisation group equations for this effective operator have been derived in the context of the four-dimensional SM and MSSM [30, 31].

In the present case we consider the effective neutrino mass operator with dimensional coupling  $\tilde{k}_{ij}$ ; after spontaneous symmetry breaking, the Majorana neutrino masses can be written as  $m_\nu \equiv kv^2 \sin^2 \beta$  ( $v$  being the vev of the Higgs field and  $\tan \beta$ , the ratio of the vevs of our two Higgs doublets) and  $k = \tilde{k}_{ij}/(2M\pi R)$  for bulk propagating, and  $k = \tilde{k}/(2M)$  for brane localised matter superfield scenarios respectively.

As such, we have set  $M_Z$  as the renormalisation point, and use  $t = \ln(\frac{\mu}{M_Z})$  and  $S(t) = e^t M_Z R$ . The general form of evolution equations for Yukawa couplings and neutrino  $k$  coupling at the one loop can be written in the following form Refs [43–45]

:

$$\begin{aligned} 16\pi^2 \frac{dY_d}{dt} &= Y_d \left\{ T_t C_1 - G_d + \frac{3}{2}(Y_d^\dagger Y_d - Y_u^\dagger Y_u) C_2 \right\}, \\ 16\pi^2 \frac{dY_u}{dt} &= Y_u \left\{ T_t C_1 - G_u + \frac{3}{2}(Y_u^\dagger Y_u - Y_d^\dagger Y_d) C_2 \right\}, \\ 16\pi^2 \frac{dY_e}{dt} &= Y_e \left\{ T_t C_1 - G_e + \frac{3}{2}(Y_e^\dagger Y_e) C_2 \right\}, \\ 16\pi^2 \frac{dk}{dt} &= \alpha k + \left( [Y_e^T Y_e^*] k + k [Y_e^\dagger Y_e] \right) C_3. \end{aligned} \quad (22)$$

where  $T_t = Tr[3Y_d^\dagger Y_d + 3Y_u^\dagger Y_u + Y_e^\dagger Y_e]$ .

### 5.1. Standard Model

The SM is a limiting case for the UED, where the KK states decouple. The coefficients in the evolution equation are defined by:

$$\begin{aligned} G_{dSM} &= \left( \frac{1}{4}g_1^2 + \frac{9}{4}g_2^2 + 8g_3^2 \right), \\ G_{uSM} &= \left( \frac{17}{20}g_1^2 + \frac{9}{4}g_2^2 + 8g_3^2 \right), \\ G_{eSM} &= \left( \frac{9}{4}g_1^2 + \frac{9}{4}g_2^2 \right), \\ \alpha_{SM} &= 2 T_t - 3g_2^2 + \lambda, \\ C_{1SM} &= 1, \\ C_{2SM} &= 1, \\ C_{3SM} &= -\frac{3}{2}. \end{aligned} \quad (23)$$

Note that there is a difference in the coefficients of the gauge coupling  $g_1$  between Ref [43]. and Ref [44]. due to the  $SU(5)$  normalisation factor  $3/5$ .

### 5.2. UED SM Bulk

The UED contribution is obtained when KK states enter, where due to the orbifolding the zero mode for fermions are chiral, which are replaced by Dirac fermions at each KK level. This lead to the factor 2 appearing in  $C_1$  and  $C_2$  since the KK left and right- handed chiral states contribute to the closed fermion one loop diagrams. That is,

$$\begin{aligned}
G_{dUEDBulk} &= \left( \frac{17}{120}g_1^2 + \frac{15}{8}g_2^2 + \frac{28}{3}g_3^2 \right) (S(t) - 1) , \\
G_{uUEDBulk} &= \left( \frac{101}{120}g_1^2 + \frac{15}{8}g_2^2 + \frac{28}{3}g_3^2 \right) (S(t) - 1) , \\
G_{eUEDBulk} &= \left( \frac{99}{40}g_1^2 + \frac{15}{8}g_2^2 \right) (S(t) - 1) , \\
\alpha_{UEDBulk} &= (S(t) - 1) \left( 4T_t - \frac{3}{20}g_1^2 - \frac{11}{4}g_2^2 + \lambda \right) , \\
C_{1UEDBulk} &= 2(S(t) - 1) , \\
C_{2UEDBulk} &= (S(t) - 1) , \\
C_{3UEDBulk} &= (S(t) - 1) .
\end{aligned} \tag{24}$$

Following the convention of Ref [15]. we use the coefficient  $(S(t) - 1) = (\mu R - 1)$ , which depends on the energy scale and also lead to a reproduction of the SM before crossing the threshold of the first KK state at  $\mu = 1/R$ . This coefficient corresponds to  $s = \frac{\mu}{\mu_0}$  for the UED case only in Ref [43].

### 5.3. UED SM Brane

For the case where the fermions are restricted to the brane, we obtain the coefficients from Ref [33]. and Ref [43]. with a difference related to the  $SU(5)$  normalisation factor:

$$\begin{aligned}
G_{dUEDBrane} &= \left( \frac{1}{4}g_1^2 + \frac{9}{4}g_2^2 + 8g_3^2 \right) 2(S(t) - 1) , \\
G_{uUEDBrane} &= \left( \frac{17}{20}g_1^2 + \frac{9}{4}g_2^2 + 8g_3^2 \right) 2(S(t) - 1) , \\
G_{eUEDBrane} &= \left( \frac{9}{4}g_1^2 + \frac{9}{4}g_2^2 \right) 2(S(t) - 1) , \\
\alpha_{UEDBrane} &= 2(S(t) - 1) \left( -3g_2^2 + \lambda \right) , \\
C_{1UEDBrane} &= 0 , \\
C_{2UEDBrane} &= 2(S(t) - 1) , \\
C_{3UEDBrane} &= 2(S(t) - 1) .
\end{aligned} \tag{25}$$

Note that the coefficient  $C_1 = 0$  since we do not have a trace of fermionic loops as the fermions are restricted to the brane.

## 6. Yukawa evolutions in the MSSM and 5D MSSM

In the following we write the general form of the evolution equations for the various MSSMs we shall consider here, where we shall use a notation similar to the ones of Refs [18, 45]. Note that the beta functions contain terms quadratic in the cut-off, where this part dominates the evolution of the Yukawa couplings and of  $k$ . The top Yukawa coupling becomes non-perturbative before the gauge couplings thus limiting the range of validity of the effective theory.

$$\begin{aligned}
16\pi^2 \frac{dY_d}{dt} &= Y_d \left\{ T_d \tilde{C} - G_d + (3Y_d^\dagger Y_d + Y_u^\dagger Y_u) C \right\} , \\
16\pi^2 \frac{dY_u}{dt} &= Y_u \left\{ T_u \tilde{C} - G_u + (3Y_u^\dagger Y_u + Y_d^\dagger Y_d) C \right\} , \\
16\pi^2 \frac{dY_e}{dt} &= Y_e \left\{ T_e \tilde{C} - G_e + (3Y_e^\dagger Y_e) C \right\} , \\
16\pi^2 \frac{dk}{dt} &= \alpha k + \left( [Y_e^T Y_e^*] k + k [Y_e^\dagger Y_e] \right) C .
\end{aligned} \tag{26}$$

where

$$\begin{aligned}
T_d &= 3 \operatorname{Tr}(Y_d^\dagger Y_d) + \operatorname{Tr}(Y_e^\dagger Y_e) , \\
T_u &= 3 \operatorname{Tr}(Y_u^\dagger Y_u) , \\
T_e &= 3 \operatorname{Tr}(Y_d^\dagger Y_d) + \operatorname{Tr}(Y_e^\dagger Y_e) .
\end{aligned} \tag{27}$$

### 6.1. MSSM

The MSSM, as a limiting case of the 5D models we shall consider in the following, and also when  $0 < t < \ln(\frac{1}{M_Z R})$  (that is the energy we consider for the evolution from  $M_Z$  to  $1/R$ ) the coefficients in the evolution equations are:

$$\begin{aligned}
G_{dMSSM} &= \left( \frac{7}{15} g_1^2 + 3g_2^2 + \frac{16}{3} g_3^2 \right) , \\
G_{uMSSM} &= \left( \frac{13}{15} g_1^2 + 3g_2^2 + \frac{16}{3} g_3^2 \right) , \\
G_{eMSSM} &= \left( \frac{9}{5} g_1^2 + 3g_2^2 \right) , \\
\alpha_{MSSM} &= 2 T_u - \frac{6}{5} g_1^2 - 6g_2^2 , \\
C_{MSSM} &= 1 , \\
\tilde{C}_{MSSM} &= 1 .
\end{aligned} \tag{28}$$

These coefficients are modified when we enter the energy regime where the effects of the extra dimensions set in. The modifications depend on which particles are

decoupled and on the structure of the model. We shall consider two cases, one in which all particles can propagate in the extra dimensions (bulk case) and the other in which fermionic matter fields are constrained to the brane (brane case).

### 6.2. Bulk

When the energy scale  $E > 1/R$  or when the energy scale parameter  $t > \ln(\frac{1}{M_Z R})$ , the coefficients in the 5D MSSM, for all three generations propagating in the bulk, can be expressed as:

$$\begin{aligned}
G_{d5Dbulk} &= \left( \frac{7}{15}g_1^2 + 3g_2^2 + \frac{16}{3}g_3^2 \right) S(t) , \\
G_{u5Dbulk} &= \left( \frac{13}{15}g_1^2 + 3g_2^2 + \frac{16}{3}g_3^2 \right) S(t) , \\
G_{e5Dbulk} &= \left( \frac{9}{5}g_1^2 + 3g_2^2 \right) S(t) , \\
\alpha_{5Dbulk} &= 2\tilde{C}_{5Dbulk}T_u - \left( \frac{6}{5}g_1^2 + 6g_2^2 \right) S(t) , \\
C_{5Dbulk} &= \pi S(t)^2 , \\
\tilde{C}_{5Dbulk} &= \pi S(t)^2 .
\end{aligned} \tag{29}$$

### 6.3. Brane

However, when all matter superfields are constrained to live on the 4D brane, the quadratic evolution due to the sum over the two KK towers will be milder. We note also that the traces are the same in the MSSM because we don't have a fermionic loop in the extra- dimension in the brane case. The coefficients of the evolution equations are given by:

$$\begin{aligned}
G_{d5Dbrane} &= \left( \frac{19}{30}g_1^2 + \frac{9}{2}g_2^2 + \frac{32}{3}g_3^2 \right) S(t) , \\
G_{u5Dbrane} &= \left( \frac{43}{30}g_1^2 + \frac{9}{2}g_2^2 + \frac{32}{3}g_3^2 \right) S(t) , \\
G_{e5Dbrane} &= \left( \frac{33}{10}g_1^2 + \frac{9}{2}g_2^2 \right) S(t) , \\
\alpha_{5Dbrane} &= 2 T_u - \left( \frac{9}{5}g_1^2 + 9g_2^2 \right) S(t) , \\
C_{5Dbrane} &= 2S(t) , \\
\tilde{C}_{5Dbrane} &= 1 .
\end{aligned} \tag{30}$$



## 7. Scaling of the Yukawa couplings and the CKM matrix

It is well known that in the SM, the quark sector's flavor mixing is parameterised by the CKM matrix:

$$V_{CKM} = \begin{pmatrix} V_{ud} & V_{us} & V_{ub} \\ V_{cd} & V_{cs} & V_{cb} \\ V_{td} & V_{ts} & V_{tb} \end{pmatrix} = \begin{pmatrix} V_{11} & V_{12} & V_{13} \\ V_{21} & V_{22} & V_{23} \\ V_{31} & V_{32} & V_{33} \end{pmatrix}, \quad (31)$$

which makes it possible to explain all flavor changing weak decay processes and CP-violating phenomena to date, where the 10 year run of Babar at SLAC and the Belle detector at KEK has greatly improved our knowledge of the CKM matrix elements. In particular, for the standard parameterisation of the CKM matrix, which has the form:

$$V_{CKM} = \begin{pmatrix} c_{12}c_{13} & s_{12}c_{13} & s_{13}e^{-i\delta} \\ -s_{12}c_{23} - c_{12}s_{23}s_{13}e^{i\delta} & c_{12}c_{23} - s_{12}s_{23}s_{13}e^{i\delta} & s_{23}c_{13} \\ s_{12}s_{23} - c_{12}c_{23}s_{13}e^{i\delta} & -c_{12}s_{23} - s_{12}c_{23}s_{13}e^{i\delta} & c_{23}c_{13} \end{pmatrix}, \quad (32)$$

where  $s_{12} = \sin \theta_{12}$ ,  $c_{12} = \cos \theta_{12}$  etc. are the sines and cosines of the three mixing angles  $\theta_{12}$ ,  $\theta_{23}$  and  $\theta_{13}$ , and  $\delta$  is the CP violating phase.

The CKM matrix arises from a consideration of the square of the quark Yukawa coupling matrices being diagonalised by using two unitary matrices  $U$  and  $V$ ,

$$\begin{aligned} \text{diag}(f_u^2, f_c^2, f_t^2) &= U Y_u^\dagger Y_u U^\dagger, \\ \text{diag}(h_d^2, h_s^2, h_b^2) &= V Y_d^\dagger Y_d V^\dagger, \end{aligned} \quad (33)$$

in which  $f_u^2, f_c^2, f_t^2$  and  $h_d^2, h_s^2, h_b^2$  are the eigenvalues of  $Y_u^\dagger Y_u$  and  $Y_d^\dagger Y_d$  respectively. It follows that the CKM matrix appears as a result of the transition from the quark flavor eigenstates to the quark mass eigenstates upon this diagonalisation of the quark mass matrices:

$$V_{CKM} = UV^\dagger. \quad (34)$$

From the full set of one-loop coupled RGE for the Yukawa couplings and the CKM matrix, together with those for the gauge coupling equations, one can obtain the renormalisation group flow of all observables related to up- and down-quark masses and the CKM matrix elements.

The RGEs are very important tools to show the properties of the quark masses and the CKM matrix at different energy scales. We write down the general form for the evolution of  $f_i^2, h_j^2$  and the variation of each element of the CKM matrix  $V_{ik}$  [15, 23, 33] in the SM, the UED SM, the MSSM and the 5D MSSM.

### 7.1. SM, UED Bulk SM and UED Brane SM

$$\begin{aligned}
16\pi^2 \frac{df_i^2}{dt} &= f_i^2 [2(T_u A - G_u) + 3B f_i^2 - 2B \sum_j h_j^2 |V_{ij}|^2], \\
16\pi^2 \frac{dh_j^2}{dt} &= h_j^2 [2(T_d A - G_d) + 3B h_j^2 - 2B \sum_i f_i^2 |V_{ij}|^2], \\
16\pi^2 \frac{dy_e^2}{dt} &= y_e^2 [2(T_e A - G_e) + 3B y_e^2], \\
16\pi^2 \frac{dV_{ik}}{dt} &= -\frac{3}{2} B \left[ \sum_{m,j \neq i} \frac{f_i^2 + f_j^2}{f_i^2 - f_j^2} h_m^2 V_{im} V_{jm}^* V_{jk} + \sum_{j,m \neq k} \frac{h_k^2 + h_m^2}{h_k^2 - h_m^2} f_j^2 V_{jm}^* V_{jk} V_{im} \right],
\end{aligned} \tag{35}$$

where  $A = B = 1$  in the SM,  $A = 2S(t) - 1$ ,  $B = S(t)$  in the UED Bulk SM and  $A = 0$ ,  $B = 2S(t)$  in the UED Brane SM. The gauge couplings  $G$  for the SM, the UED Bulk SM and the UED Brane SM are written in Eq.(23), Eq.(24) and Eq.(25) respectively.

### 7.2. MSSM, 5D bulk and 5D brane

$$\begin{aligned}
16\pi^2 \frac{df_i^2}{dt} &= f_i^2 [2(T_u \tilde{C} - G_u) + 6C f_i^2 + 2C \sum_j h_j^2 |V_{ij}|^2] \\
16\pi^2 \frac{dh_j^2}{dt} &= h_j^2 [2(T_d \tilde{C} - G_d) + 6C h_j^2 + 2C \sum_i f_i^2 |V_{ij}|^2], \\
16\pi^2 \frac{dy_e^2}{dt} &= y_e^2 [2(T_e \tilde{C} - G_e) + 6C y_e^2], \\
16\pi^2 \frac{dV_{ik}}{dt} &= C \left[ \sum_{m,j \neq i} \frac{f_i^2 + f_j^2}{f_i^2 - f_j^2} h_m^2 V_{im} V_{jm}^* V_{jk} + \sum_{j,m \neq k} \frac{h_k^2 + h_m^2}{h_k^2 - h_m^2} f_j^2 V_{jm}^* V_{jk} V_{im} \right],
\end{aligned} \tag{36}$$

where we use the same forms as in Eqs.(28,29,30) to fix the coefficients  $C$ ,  $\tilde{C}$  and gauge couplings  $G$  to describe each model.

## 8. Comparison of the models and implications

In the following we compare the main results for the different models and their physical meaning both in term of experimental limits and of the theoretical implications. However, as pointed out in the Appendix, there is a subtlety involved the running of the physical parameters in the UED bulk model. Although we plot their running up to the gauge unification scale, in fact, as illustrated in Fig.27, the introduction of new ultraviolet cutoff becomes imperative due to the scalar potential stability condition, and beyond this scale new physics should appear. For further discussion and quantitative analysis in the UED bulk model, refer to Ref [46] for details. In contrast, in the UED brane model, the physics parameters have a full running till

the gauge unification scale, since the Higgs self coupling evolution has a finite value which thus excludes the vacuum stability concern and validates the theory up its full scale. [33]

### 8.1. *Top Yukawa coupling*

#### *UED SM: Bulk and Brane cases*

In Fig.4 the initial Yukawa couplings are given by the ratios of the fermion masses to the Higgs vacuum expectation value. The Yukawa couplings evolve in the usual logarithmic fashion when the energy is below 2 TeV, 8 TeV, and 15 TeV for the three different cases. However, once the first KK threshold is reached, the contributions from the KK states become more and more significant. The evolution of  $f_t$  (see Eq.(35)) depends explicitly on the cutoff  $\Lambda$ , which have finite one-loop corrections to the beta functions at each massive KK excitation level. Therefore, the running of the Yukawa couplings, or more precisely, the one-loop KK corrected effective four dimensional Yukawa couplings, begins to deviate from their normal orbits and start to evolve faster and faster. For the compactification radius  $R^{-1} = 2$  TeV, the Yukawa couplings evolve faster than the other two, reaching its minimum value at the unification scale, after that point their evolution will “blow-up” due to the faster running of the gauge couplings and new physics would come into play. For the radius  $R^{-1} = 8$  TeV, we find similar behaviour to the  $R^{-1} = 2$  TeV case, where the “blow-up” scale is not very far from that of 2 TeV case. However, for the third choice of radius, since the compactification radius is now much higher than the other two, we need more energy to push it further toward its “blow-up” point, which is at a higher unification scale. We also observe that the Yukawa couplings are quickly evolving to zero, however, a satisfactory unification of these seems to still be lacking. In the UED scenario, the unification of the Yukawa couplings is very desirable due to the fast power law running. As such, we have so far observed the Yukawa couplings all decrease with increasing energy, which agrees with what is observed in the SM, however, the Yukawa couplings are driven dramatically towards extremely weak values at a much faster rate. This is an interesting feature that distinguishes the UED model from that of the SM.

#### *5D MSSM Bulk*

The 4D MSSM contains the particle spectrum of a two-Higgs doublet model extension of the SM and the corresponding supersymmetric partners. After the spontaneous breaking of the electroweak symmetry, five physical Higgs particles are left in the spectrum. The two Higgs doublets  $H_u$  and  $H_d$ , with opposite hypercharges, are responsible for the generation of the up-type and down-type quarks respectively. The vacuum expectation values of the neutral components of the two Higgs fields satisfy the relation  $v_u^2 + v_d^2 = \left(\frac{246}{\sqrt{2}}\right)^2 = (174\text{GeV})^2$ . The fermion mass matrices appear after the spontaneous symmetry breaking from the fermion-Higgs Yukawa

couplings. As a result, the initial Yukawa couplings are given by the ratios of the fermion masses to the appropriate Higgs vacuum expectation values as follows:

$$f_{u,c,t} = \frac{m_{u,c,t}}{v_u} \quad , \quad h_{d,s,b} = \frac{m_{d,s,b}}{v_d} \quad , \quad y_{e,\mu,\tau} = \frac{m_{e,\mu,\tau}}{v_d} \quad , \quad (37)$$

where we define  $\tan \beta = v_u/v_d$ , which is the ratio of vacuum expectation values of the two Higgs fields  $H_u$  and  $H_d$ .

From the complete sets of the RGEs we can run the renormalisation group flow of all observables related to up- and down-quark masses and the quark flavor mixings. For our numerical analysis we assume the fundamental scale is not far from the range of LHC scale, and set the compactification scale to be  $R^{-1} = 2$  TeV, 8 TeV, and 15 TeV respectively.

Actually, below the supersymmetric breaking scale the Yukawa and gauge couplings run in the usual logarithmic fashion, giving a rather slow change for their values. Therefore, for supersymmetric breaking theories around TeV scales, for simplicity, we take the supersymmetric breaking scale  $M_{SUSY} = M_Z$  in the present numerical study, and run the RGEs from  $M_Z$  up to the high energy scales for our three different compactification scales.

Additionally, as illustrated in Fig. 5, for the case of universal 5D MSSM, once the first KK threshold is crossed at  $\mu = R^{-1}$ , the power law running of the various beta functions causes the Yukawa coupling to rapidly increase following the rapid increase in the gauge coupling constants in the left panel of Fig.3. From Eq.(36) and Eq.(29) we can find the quadratic term of  $S(t)$  providing a positive contribution to the Yukawa beta functions, which is in contrast to beta functions of the gauge couplings (which include terms only linear in  $S(t)$ ). Therefore, from Eq.(36), the positive contribution from  $S(t)$  terms will dominate the negative contributions from the gauge couplings, and cause the Yukawa couplings to increase rapidly. This behaviour can be observed for both small and large  $\tan \beta$  cases. However, as illustrated in the first graph of Fig. 5, for small  $\tan \beta$ , the Yukawa coupling has a

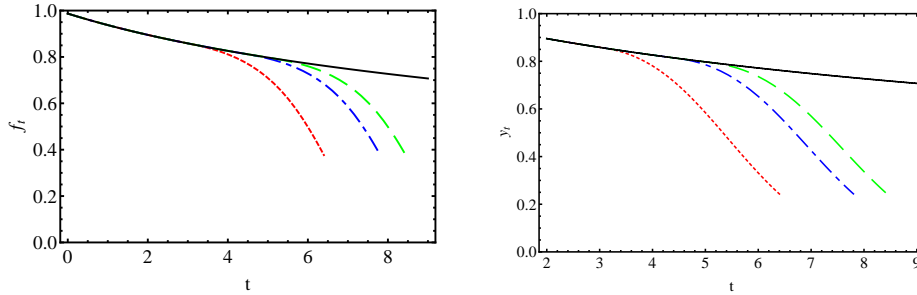


Fig. 4. The Yukawa coupling  $f_t$  for the top quark in the UED SM as a function of the scale parameter  $t$ , for the bulk case (left panel) and the brane case (right panel) where the solid line is the SM evolution and for different compactification scales:  $R^{-1} = 2$  TeV (red, dotted line), 8 TeV (blue, dot-dashed line), and 15 TeV (green, dashed line).

large initial value, therefore it blows up at a relatively low energy as compared with the case for large  $\tan\beta$ . As a result, as one evolves upward in the scale, the top Yukawa coupling is rising with a fast rate and is pushed up against the Landau pole where it becomes divergent and blows up. In the vicinity of this singular point the perturbative calculation becomes invalid, and the higher order corrections become significant. The Landau pole also indicates that there is an upper limit on the value of the gauge couplings where new physics must emerge before the Yukawa couplings diverge.

### 5D MSSM Brane

In the brane localised matter field scenario, the beta function has only linear terms in  $S(t)$ , which is comparable with the  $S(t)$  term in the beta function for the gauge couplings. As depicted in Fig. 6, for a small value of  $\tan\beta$ , we have a large initial value of  $f_t$  and the gauge coupling contribution to the Yukawa beta function is subdominant only. Therefore, as discussed previously, the Yukawa coupling  $f_t$  increases rapidly as one crosses the KK threshold at  $\mu = R^{-1}$ , resulting in a rapid approach of the singularity before the unification scale is reached. However, for an intermediate value of  $\tan\beta$ , we have a relative smaller initial condition for the top Yukawa coupling and the Yukawa terms in the beta function become less important. The contributions from the gauge couplings may then become significant, which leads to a net negative contribution to the beta functions. Therefore, the curvature of the trajectory of the top Yukawa evolution might change direction, and the Yukawa evolution will decrease instead of increasing. This behaviour would become more obvious for a large value of  $\tan\beta$ . As observed in Fig. 6, for  $\tan\beta = 30$ , we indeed observe the decreasing behaviour of the top Yukawa couplings. This behaviour provides a very clear phenomenological signature, especially for scenarios with a larger  $\tan\beta$  and that are valid up to the unification scale where the gauge couplings

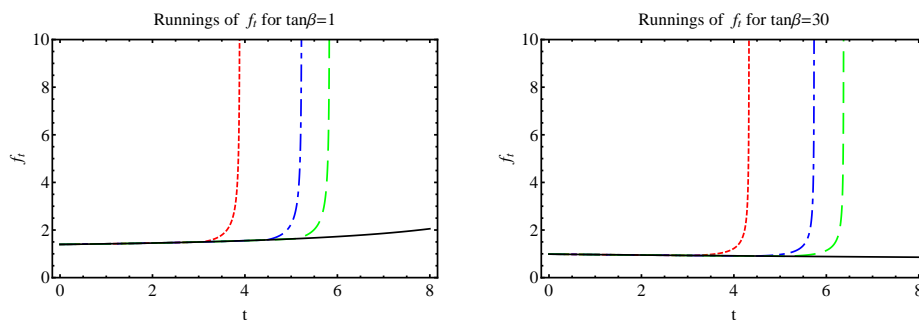


Fig. 5. The Yukawa coupling  $f_t$  for the top quark in the bulk case of 5D MSSM as a function of the scale parameter  $t$ , for (left panel)  $\tan\beta = 1$  and (right panel)  $\tan\beta = 30$  where the solid line is the MSSM evolution and for different compactification scales:  $R^{-1} = 2$  TeV (red, dotted line), 8 TeV (blue, dot-dashed line), and 15 TeV (green, dashed line).

converge.

## 8.2. CKM Matrix

Because of the arbitrariness in choice of phases of the quark fields, the phases of individual matrix elements of the  $V_{CKM}$  are not themselves directly observable. Among these we therefore use the absolute values of the matrix element  $|V_{ij}|$  as the independent set of rephasing invariant variables. Of the nine elements of the CKM matrix, only four of them are independent, which is consistent with the four independent variables of the standard parameterisation of the CKM matrix. For definiteness we choose the  $|V_{ub}|$ ,  $|V_{cb}|$ ,  $|V_{us}|$  and the Jarlskog rephasing invariant parameter  $J = \text{Im}V_{ud}V_{cs}V_{us}^*V_{cd}^*$  as the four independent parameters of  $V_{CKM}$ .

### UED SM

In Fig.7 we specially plot the evolution of  $|V_{ub}|$  for the UED bulk and brane cases. For the evolution of  $|V_{cb}|$  and  $|V_{us}|$  we can observe similar behaviours, i.e., they all increase with the energy scale; the variation rate become faster once the KK threshold is passed. The absolute values of all the remaining magnitudes of the CKM matrix elements can be obtained from the unitarity equations, as depicted in Fig.7, with increasing energy the running of the CKM matrix shows a pronounced pattern at the point where the KK modes are excited, thus we could determine the renormalisation group evolutions of the full CKM matrix. As can be seen from Eq.(35), the evolution of the CKM matrix is governed by the Yukawa couplings and the factor  $S(t)$ . They evolve faster in the region where the power law scaling of the Yukawa couplings becomes substantial. Therefore, the renormalisation effect is explicit for mixings involving the third family, i.e.,  $|V_{ub}|$  and  $|V_{cb}|$ , due to the large value of their Yukawa coupling. Because of the smallness of the Yukawa coupling

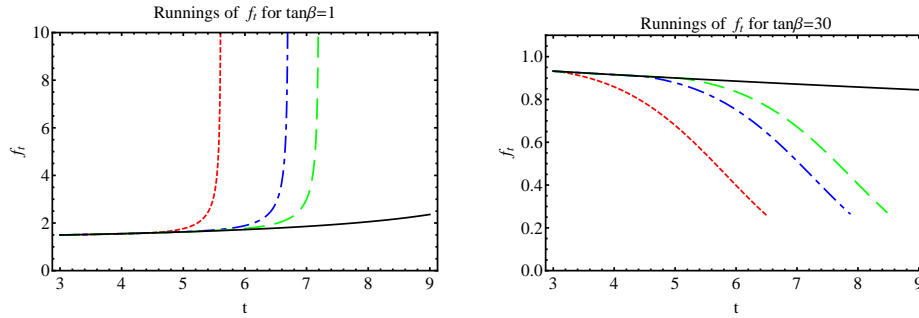


Fig. 6. The Yukawa coupling  $f_t$  for the top quark in the brane case of 5D MSSM as a function of the scale parameter  $t$ , for (left panel)  $\tan \beta = 1$  and (right panel)  $\tan \beta = 30$  where the solid line is the MSSM evolution and for different compactification scales:  $R^{-1} = 2$  TeV (red, dotted line), 8 TeV (blue, dot-dashed line), and 15 TeV (green, dashed line).

terms, the renormalisation group flow of the mixing between the first two families, i.e., the Cabibbo angle of  $|V_{us}|$ , turns out to be very small. Although the mixing angle increases all the time, it is rather inert, even in the UED model.

### 5D MSSM

In Figs.8 and 9 we plot the energy dependence of  $|V_{ub}|$  from the weak scale all the way up to the high energy scales for different values of compactification radii  $R^{-1}$  for the bulk 5D MSSM case brane localised matter fields case respectively. In these sets of pictures we consider two indicative choices of  $\tan\beta$ , that of  $\tan\beta = 1$  and  $\tan\beta = 30$ .

The running of the CKM matrix is governed by the terms related to the Yukawa couplings. These Yukawa couplings are usually very small, except for the top Yukawa coupling (which could give a sizeable contribution). The CKM matrix element  $V_{ub} \simeq \theta_{13}e^{-i\delta}$  can be used to observe the mixing angle,  $\theta_{13}$ . It decreases with the energy scale in a similar manner regardless of whether  $\tan\beta$  is small or large. However, for a large initial value of  $f_t$  (small  $\tan\beta$ ), the mixing angles have a more rapid evolution and end in the regime where the top Yukawa diverges and develops a singularity. Quantitatively we observe from these plots that the value of  $|V_{ub}|$  change by more than 50%.

### 8.3. The Jarlskog parameter

#### UED SM

We next turn our attention to the quark flavor mixing matrix, especially the complex phase of the CKM matrix which characterises CP-violating phenomena. This phenomena has been unambiguously verified in a number of  $K - \bar{K}$  and  $B - \bar{B}$  systems. For the parameter  $J$  (Fig.10), the characteristic parameter for the CP non-conservation effects, its variation becomes very significant. The larger the value

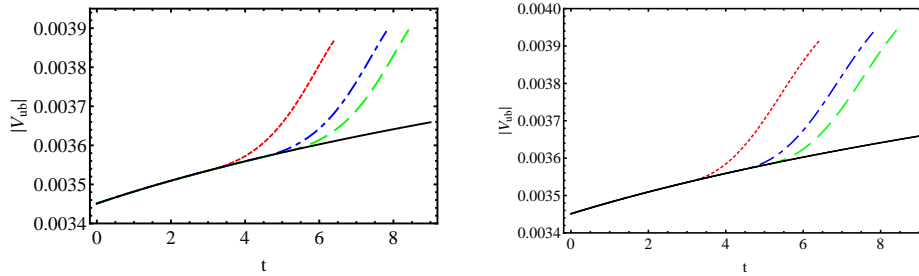


Fig. 7. The CKM matrix elements  $|V_{ub}|$  in the UED SM as a function of the scale parameter  $t$ , for the bulk case (left panel) and the brane case (right panel) where the solid line is the SM, for different compactification scales:  $R^{-1} = 2$  TeV (red, dotted line), 8 TeV (blue, dot-dashed line), and 15 TeV (green, dashed line).

of the compactification radius  $R$ , the faster  $J$  evolves to reach its maximum. We observe an approximate 30% increase for  $J$  at the unification scale compared with its initial value.

### 5D MSSM

From Figs.11, in contrast, the Jarlskog parameter decreases quite rapidly once the initial KK threshold is passed. However, when  $\tan \beta$  is large, we have a relatively longer distance between the initial and terminating energy track, the evolution of  $J$  can be driven towards zero or even further. Besides, as can be seen explicitly in Ref [32]., the beta functions of the evolution equations of the CKM elements are up to the third order of the CKM elements, which are comparable smaller than that of Jarlskog parameter's quadratic dependence on the CKM elements. This fact then

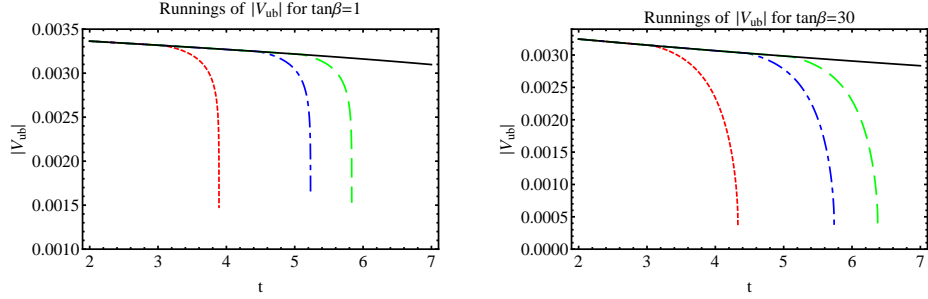


Fig. 8. The CKM matrix elements  $|V_{ub}|$  in the bulk case of 5D MSSM as a function of the scale parameter  $t$ , for (left panel)  $\tan \beta = 1$  and (right panel)  $\tan \beta = 30$  where the solid line is the MSSM evolution and for different compactification scales:  $R^{-1} = 2$  TeV (red, dotted line), 8 TeV (blue, dot-dashed line), and 15 TeV (green, dashed line).

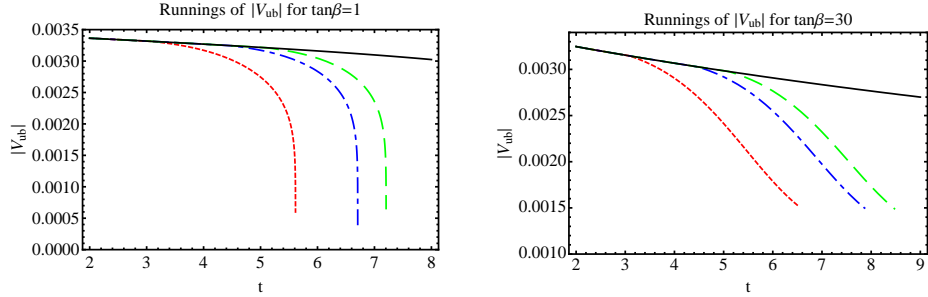


Fig. 9. The CKM matrix elements  $|V_{ub}|$  in the brane case of 5D MSSM as a function of the scale parameter  $t$ , for (left panel)  $\tan \beta = 1$  and (right panel)  $\tan \beta = 30$  where the solid line is the MSSM evolution and for different compactification scales:  $R^{-1} = 2$  TeV (red, dotted line), 8 TeV (blue, dot-dashed line), and 15 TeV (green, dashed line).



leads to the relatively large variation of  $J$  with the increase of energy. Furthermore, for  $\tan \beta = 30$ , the Jarlskog parameter drops almost to zero, which sets the effect of the SM CP violation to being very small. Note, however, that in a supersymmetric theory other sources of CP violation beyond the SM ones are typically present, therefore only a complete and detailed study of a specific model would allow us to establish the strength of the CP violating effects.

For the matter fields constrained to the brane, in Figs.9 and 12 we observe that the evolutions of these mixing angles and CP violation parameter are decreasing irrespective of whether the top Yukawa coupling grows or not. For small  $\tan \beta$  we see similar evolution behaviours for these parameters as in the bulk case. The decreases in the value of  $V_{ub}$  and  $J$  are much steeper, due to rapid growth of the top Yukawa coupling near the singular point. However, as  $\tan \beta$  becomes larger, e.g.  $\tan \beta = 30$ , the top Yukawa coupling evolves downward instead of upward. The decreases in these CKM parameters then becomes much milder towards the unification scale; though the reduction to effectively zero in the Jarlskog parameter persists. As a result, for the brane localised matter field scenario, it is more desirable to have a large  $\tan \beta$  for theories that are valid up to the gauge coupling unification scale.

In summary, for the two 5D MSSM scenarios with matter fields in the bulk or on the brane, we have performed the numerical analysis of the evolution of the various parameters of the CKM matrix, and both cases give us a scenario with small or no quark flavor mixings at high energies, especially for the mixings with the heavy generation. The evolution equations which relate various observables at different energies, and also allow the study of their asymptotic behaviours, are particularly important in view of testing the evolution of the Yukawa couplings. In the universal 5D MSSM model, the evolution of these CKM parameters have a rapid variation prior to reaching a cut-off scale where the top Yukawa coupling develops a singularity point and the model breaks down. For the brane localised matter fields model, we can only observe similar behaviours for small values of  $\tan \beta$ , while for large  $\tan \beta$ , the initial top Yukawa coupling becomes smaller, the gauge couplings then play

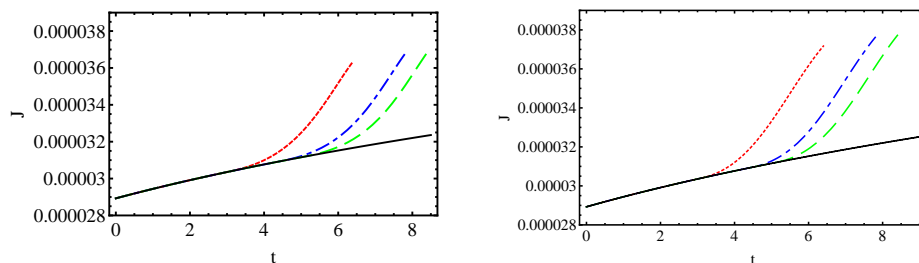


Fig. 10. The Jarlskog parameter  $J$  in the UED SM as a function of the scale parameter  $t$ , for the bulk case (left panel) and the brane case (right panel) where the solid line is the SM, for different compactification scales:  $R^{-1} = 2$  TeV (red, dotted line), 8 TeV (blue, dot-dashed line), and 15 TeV (green, dashed line).

a dominant role during the evolution of the Yukawa couplings, which cause the Yukawa couplings to decrease instead of increasing. As such the variations of these CKM parameters have a relatively milder behaviour, and the theory is valid up the gauge coupling unification scale.

### 9. Neutrino parameter evolutions

In a similar way to what done for quark parameters, we can study the evolution of the masses, mixing and phases in the neutrino sector. In the following we first establish our conventions for these parameters and introduce the main present bounds and values from experiments. We then introduce the corresponding renormalisation evolution equations in the various models and discuss the numerical values obtained for the evolution of the parameters in different models, as previously done for the quark sector.

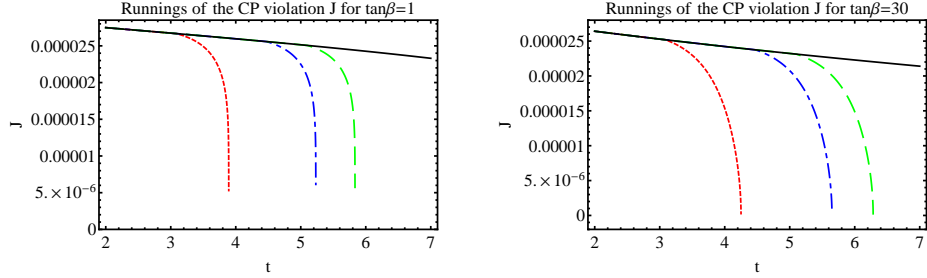


Fig. 11. The Jarlskog parameter  $J$  in the bulk case of 5D MSSM as a function of the scale parameter  $t$ , for (left panel)  $\tan \beta = 1$  and (right panel)  $\tan \beta = 30$  where the solid line is the MSSM evolution and for different compactification scales:  $R^{-1} = 2$  TeV (red, dotted line), 8 TeV (blue, dot-dashed line), and 15 TeV (green, dashed line).

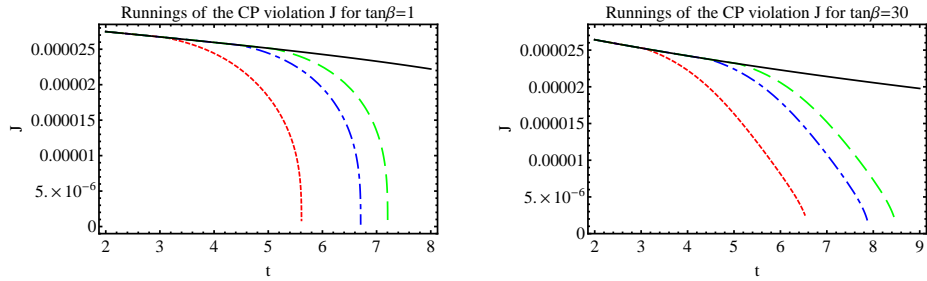


Fig. 12. The Jarlskog parameter  $J$  in the brane case of 5D MSSM as a function of the scale parameter  $t$ , for (left panel)  $\tan \beta = 1$  and (right panel)  $\tan \beta = 30$  where the solid line is the MSSM evolution and for different compactification scales:  $R^{-1} = 2$  TeV (red, dotted line), 8 TeV (blue, dot-dashed line), and 15 TeV (green, dashed line).

### 9.1. Conventions for masses and mixing parameters

The mixing matrix which relates gauge and mass eigenstates is defined to diagonalise the neutrino mass matrix in the basis where the charged lepton mass matrix is diagonal. It is usually parameterised as follows [47]:

$$U = \begin{pmatrix} c_{12}c_{13} & s_{12}c_{13} & s_{13}e^{-i\delta} \\ -s_{12}c_{23} - c_{12}s_{23}s_{13}e^{-i\delta} & c_{12}c_{23} - s_{12}s_{23}s_{13}e^{i\delta} & s_{23}c_{13} \\ s_{12}s_{23} - c_{12}c_{23}s_{13}e^{i\delta} & -c_{12}s_{23} - s_{12}c_{23}s_{13}e^{i\delta} & c_{23}c_{13} \end{pmatrix} \begin{pmatrix} e^{i\phi_1} & & \\ & e^{i\phi_2} & \\ & & 1 \end{pmatrix},$$

with  $c_{ij} = \cos \theta_{ij}$  and  $s_{ij} = \sin \theta_{ij}$  ( $ij = 12, 13, 23$ ). We follow the conventions of Ref. [45] to extract mixing parameters from the PMNS matrix.

Experimental information on neutrino mixing parameters and masses is obtained mainly from oscillation experiments. In general  $\Delta m_{atm}^2$  is assigned to a mass squared difference between  $\nu_3$  and  $\nu_2$ , whereas  $\Delta m_{sol}^2$  to a mass squared difference between  $\nu_2$  and  $\nu_1$ . The current observational values are summarised in Table 2. Data indicates that  $\Delta m_{sol}^2 \ll \Delta m_{atm}^2$ , but the masses themselves are not determined. In this work we have adopted the masses of the neutrinos at the  $M_Z$  scale as  $m_1 = 0.1$  eV,  $m_2 = 0.100379$  eV, and  $m_3 = 0.11183$  eV, as the *normal* hierarchy (whilst any reference to an *inverted* hierarchy would refer to  $m_3 = 0.1$  eV, with  $m_3 < m_1 < m_2$  and satisfying the above bounds). For the purpose of illustration, we choose values for the angles and phases as the  $M_Z$  scale as:  $\theta_{12} = 34^\circ$ ,  $\theta_{13} = 8.83^\circ$ ,  $\theta_{23} = 46^\circ$ ,  $\delta = 30^\circ$ ,  $\phi_1 = 80^\circ$  and  $\phi_2 = 70^\circ$ .

Table 2. Present limits on neutrino masses and mixing parameters used in the text. Data is taken from Ref. [48] for  $\sin^2(2\theta_{13})$ , and from Ref. [41].

Parameter	Value (90% CL)
$\sin^2(2\theta_{12})$	$0.861^{(+0.026)}_{(-0.022)}$
$\sin^2(2\theta_{23})$	$> 0.92$
$\sin^2(2\theta_{13})$	$0.092 \pm 0.017$
$\Delta m_{sol}^2$	$(7.59 \pm 0.21) \times 10^{-5} \text{ eV}^2$
$\Delta m_{atm}^2$	$(2.43 \pm 0.13) \times 10^{-3} \text{ eV}^2$

The evolution equation for the observables in our 5D MSSM are taken from [24]. As expected  $\tan \beta$  plays an important role as all the mixing angles and phases depend on  $y_\tau$  (see Appendix C in [24]). However, the new degrees of freedom (the extra-dimensional fields giving rise to KK excitations of the zero modes) become important at energies corresponding to their masses. In the following we study the evolution of the relevant parameters, such as  $\Delta m_{sol}^2$ ,  $\Delta m_{atm}^2$  and the angles and phases, as a function of the energy scale and of  $\tan \beta$ . Only some selected plots will be shown and we will comment on the other similar cases not explicitly shown.

## 9.2. $\Delta m_{sol}^2$ and $\Delta m_{atm}^2$

For the UED SM, we see different behaviour for the brane case Fig.13 and bulk case Fig. 14. Once the KK threshold is reached, both  $\Delta m_{sol}^2$  and  $\Delta m_{atm}^2$  decrease with increasing energy in the brane case, but they increase with the energy in the bulk case for the different radii of compactification. The evolution of masses depends on the evolution of  $y_\tau$  and  $k$  coupling and the RG runnings in the UED SM bulk model are generally larger than those in UED SM brane model. This is due to the fact that the coefficient  $C_1 = 0$  in the brane model (Eq.(25)) and  $2(S(t)-1)$  in the bulk model (Eq.(24)) and also there is difference in  $\alpha$  in the two equations due to the trace of charged-fermion Yukawa couplings in bulk model whereas such a contribution does

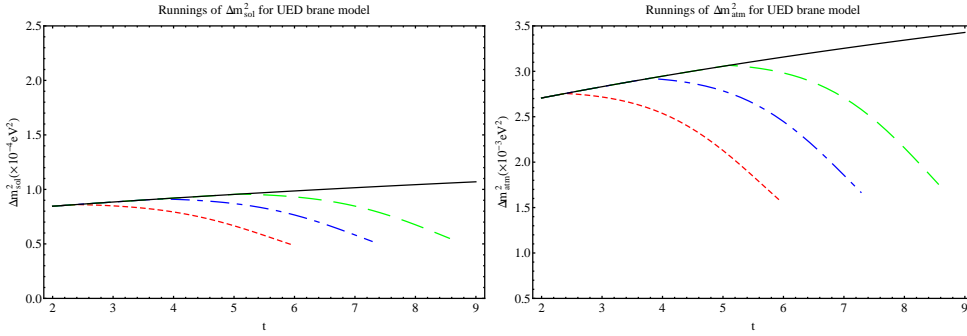


Fig. 13. Evolution of  $\Delta m_{sol}^2$  (left panel) and  $\Delta m_{atm}^2$  (right panel) as a function of the scale  $t = \ln(\mu/M_Z)$  with matter fields constrained to the brane in the UED SM. The black line is the SM evolution, the red (small dashes) is for  $R^{-1} \sim 1$  TeV, the blue (dash-dotted)  $R^{-1} \sim 4$  TeV, the green (large dashes)  $R^{-1} \sim 15$  TeV.

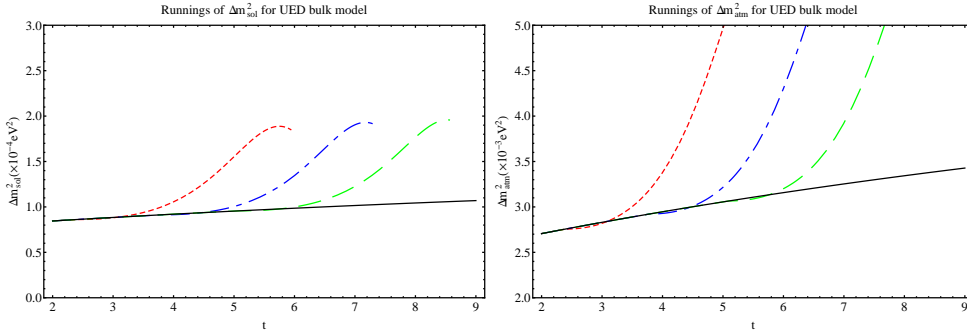


Fig. 14. Evolution of  $\Delta m_{sol}^2$  (left panel) and  $\Delta m_{atm}^2$  (right panel) as a function of the scale  $t = \ln(\mu/M_Z)$  with matter fields in the bulk in the UED SM. The black line is the SM evolution, the red (small dashes) is for  $R^{-1} \sim 1$  TeV, the blue (dash-dotted)  $R^{-1} \sim 4$  TeV, and the green (large dashes)  $R^{-1} \sim 15$  TeV.

not exist in brane model due to the absence of fermion KK excitations (see the  $T$  term in Eq.(23)). This lead to the increasing of observables in the bulk case and the decreasing in the brane case.

For the 5D MSSM, in general, in the brane case, the evolution has the same form for the three masses  $m_1, m_2, m_3$ . This leads to a reduction of up to a factor of two for the masses at  $t = 6$  (for a large radius,  $R^{-1} = 1$  TeV) with respect to the MSSM values at low energies (smaller radii give a weaker effect as the KK excitations contribute to the evolution equations at higher energies). This prediction is extremely stable and can be explained as the evolution of the masses is governed

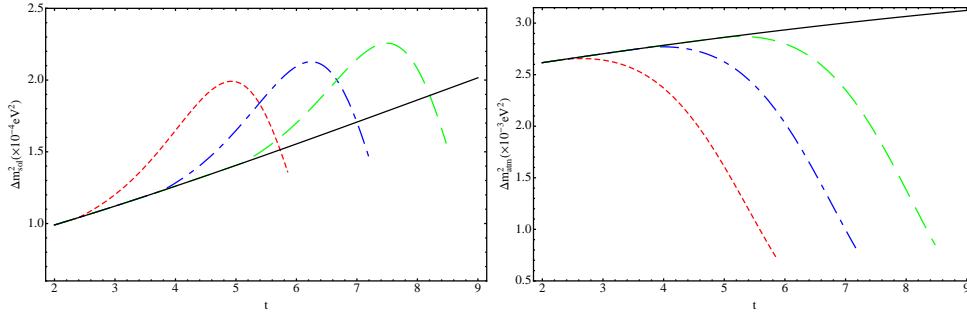


Fig. 15. Evolution of  $\Delta m_{sol}^2$  (left panel) and  $\Delta m_{atm}^2$  (right panel) as a function of the scale  $t = \ln(\mu/M_Z)$  with matter fields constrained to the brane for  $\tan \beta = 30$  in the 5D MSSM. The black line is the MSSM evolution, the red (small dashes) is for  $R^{-1} \sim 1$  TeV, the blue (dash-dotted)  $R^{-1} \sim 4$  TeV, the green (large dashes)  $R^{-1} \sim 15$  TeV.

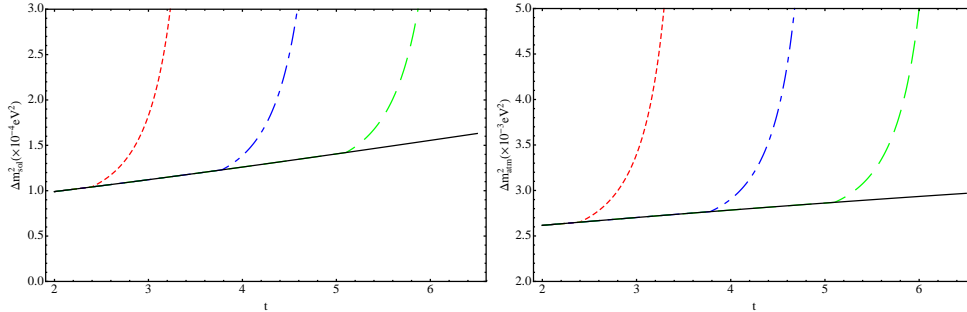


Fig. 16. Evolution of  $\Delta m_{sol}^2$  (left panel) and  $\Delta m_{atm}^2$  (right panel) as a function of the scale  $t = \ln(\mu/M_Z)$  with matter fields in the bulk for  $\tan \beta = 30$  in the 5D MSSM. The black line is the MSSM evolution, the red (small dashes) is for  $R^{-1} \sim 1$  TeV, the blue (dash-dotted)  $R^{-1} \sim 4$  TeV, and the green (large dashes)  $R^{-1} \sim 15$  TeV. The evolution is towards a non-perturbative regime, where the Yukawa coupling develops a Landau pole and the effective theory becomes invalid.

by the equation

$$\dot{m}_i = \frac{1}{16\pi^2} m_i (\alpha + C_i y_\tau^2) , \quad (38)$$

where the coefficients  $C_i$  induce a non-universal behaviour and the parameter  $\alpha$  contains the up Yukawa couplings and the gauge coupling terms (detailed in Appendix C of Ref [24]. and Eq.(30)). In contrast to the MSSM, the evolution in the brane case is completely dominated by the universal part. The essential point is that in the MSSM the positive contribution to  $\alpha$ , approximately  $6y_t^2$ , is of the same order as the negative contribution from the gauge part. In our case the gauge part has a large pre-factor  $S(t) = e^t M_Z R$  with respect to the MSSM which makes it completely dominant compared to any other contribution. As energy increases, we can write:

$$\dot{m}_i \sim \frac{1}{16\pi^2} m_i \left[ 6y_t^2 - \left( \frac{9}{5}g_1^2 + 9g_2^2 \right) S(t) \right] < 0 . \quad (39)$$

From this approximation we immediately see that all masses decrease with increasing energy and eventually tend to zero if the evolution equations can be trusted up to a high energy.

In the 5D MSSM bulk case the evolution has again the same form for the three masses  $m_1, m_2, m_3$ , but the behaviour is the opposite as the masses increase at high energy because all matter fields propagate in the bulk and contribute to the evolution. In detail this can be seen by the fact that even if the gauge part gets a large pre-factor  $S(t)$ , the Yukawa part gets in this case a pre-factor  $S(t)^2$ , which changes the sign of the derivative with respect to the previous case:

$$\dot{m}_i \sim \frac{1}{16\pi^2} m_i \left[ \pi S(t)^2 6y_t^2 - \left( \frac{6}{5}g_1^2 + 6g_2^2 \right) S(t) \right] > 0 . \quad (40)$$

From this approximation we see that all masses increase with increasing energy scale.

The situation is more involved when analysing the mass squared differences. We plot in Figs.15 and 16 the evolution of  $\Delta m_{sol}^2$  and  $\Delta m_{atm}^2$  both for the matter fields on the brane and for all fields in the bulk for  $\tan\beta=30$  and different radii of compactification. In the brane case different behaviours as a function of the energy scale are possible as a relatively large interval in energy range is allowed for the effective theory. As explicitly illustrated in Fig. 15, the relevant radiative corrections controlled by the gauge fields in Eq.(39) become dominant as energy goes up, which tends to reduce mass splitting, and an approximately degenerate neutrino masses spectrum at the high energy scale  $m_1 \approx m_2 \approx m_3$  becomes favourable. This is in contrast with the MSSM, where the neutrino mass splitting becomes large at an ultraviolet cut-off. Therefore, it is very appealing that the neutrino mass splitting at low energy could be attributed to radiative corrections resulting from a degenerate pattern at a high energy scale. In Fig.16, the bulk case tends to a non-perturbative regime, where the unitarity bounds of the effective theory are reached much faster

and only a much shorter running can be followed using the effective theory. As seen in Eq.(40), the quadratic terms related to  $S(t)$  dominate during the fast evolution. As such, the neutrino mass splitting becomes even larger at a high energy scale.

### 9.3. Mixing angles

Concerning the evolution of the mixing angles, as can be seen in Figs.17–23, in the UED bulk and brane cases, we have very small variation from the SM case because we don't have dependence on  $\tan\beta$  and there is not a quadratic term of  $S(t)$  in the RGEs so there is no strong enhancement in the running. However the mixing angles variation is more significant in the 5D MSSM in which the largest effect is for  $\theta_{12}$ , with changes of more than 70% possible for the brane localised

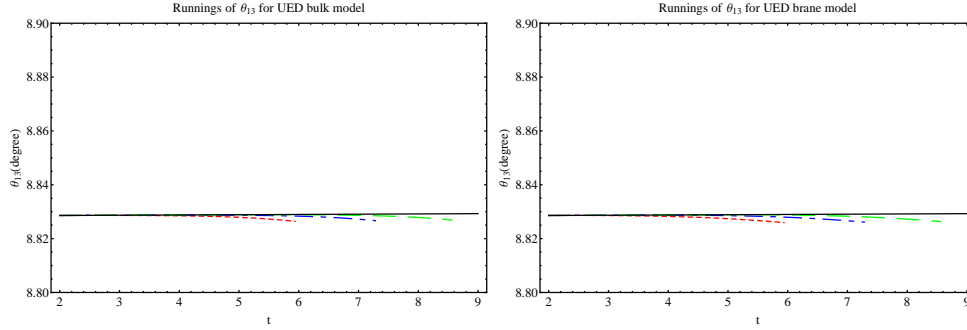


Fig. 17. Evolution of  $\theta_{13}$  as a function of the parameter  $t = \ln(\mu/M_Z)$  with matter fields in the bulk (left panel) and on the brane (right panel) respectively in the UED SM. The black line is the SM evolution, the red (small dashes) is for  $R^{-1} \sim 1$  TeV, the blue (dash-dotted)  $R^{-1} \sim 4$  TeV, and the green (large dashes)  $R^{-1} \sim 15$  TeV.

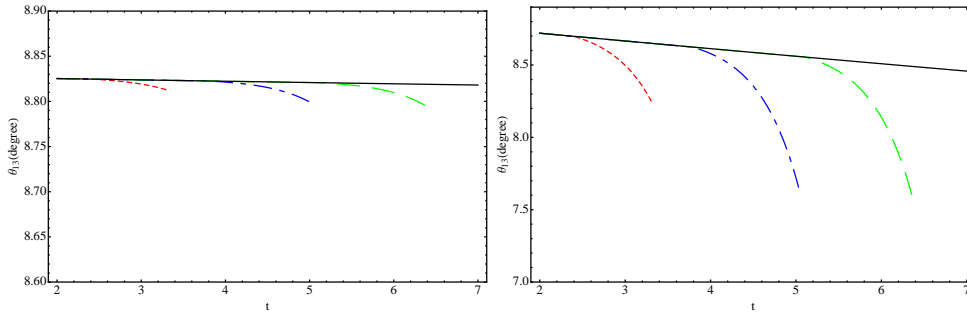


Fig. 18. Evolution of  $\theta_{13}$  as a function of the parameter  $t = \ln(\mu/M_Z)$  with matter fields in the bulk for  $\tan\beta = 5$  (left panel) and  $\tan\beta = 30$  (right panel) in the 5D MSSM respectively. The black line is the MSSM evolution, the red (small dashes) is for  $R^{-1} \sim 1$  TeV, the blue (dash-dotted)  $R^{-1} \sim 4$  TeV, and the green (large dashes)  $R^{-1} \sim 15$  TeV.

matter field scenario. As observed, due to the large quadratic term of  $S(t)$  in the beta function, the  $\theta_{12}$  has a rapid and steep variation in the bulk case. However, for the brane case, it has a relatively longer evolution track with the  $\theta_{12}$  then being pulled further down until the termination point (where the effective theory becomes invalid). In contrast, the running of  $\theta_{13}$  and  $\theta_{23}$  is much milder. As demonstrated in Figs. 18 and 19, changes in the values of  $\theta_{13}$  vary only a couple of degrees. For a larger value of  $\tan\beta$  we have a relatively large Yukawa coupling to  $\tau$ , which leads to a large magnitude for its beta function, resulting in a relatively large variation during the evolution. However, a running to  $\theta_{13} = 0$  cannot be observed in any situation. From the evolution behaviour of  $\theta_{13}$ , one can see that the renormalisation group running effects or finite quantum corrections are almost impossible to generate

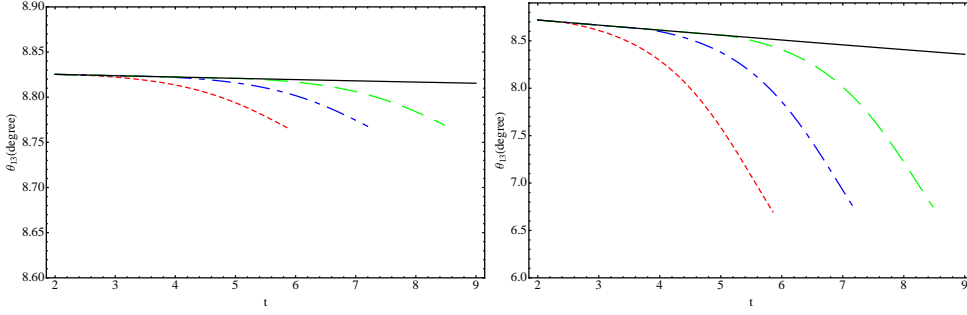


Fig. 19. Evolution of  $\theta_{13}$  as a function of the parameter  $t = \ln(\mu/M_Z)$  with matter fields constrained to the brane for  $\tan\beta = 5$  (left panel) and  $\tan\beta = 30$  (right panel) in the 5D MSSM respectively. The black line is the MSSM evolution, the red one (small dashes) is for  $R^{-1} \sim 1$  TeV, the blue (dash-dotted)  $R^{-1} \sim 4$  TeV, and the green (large dashes)  $R^{-1} \sim 15$  TeV.

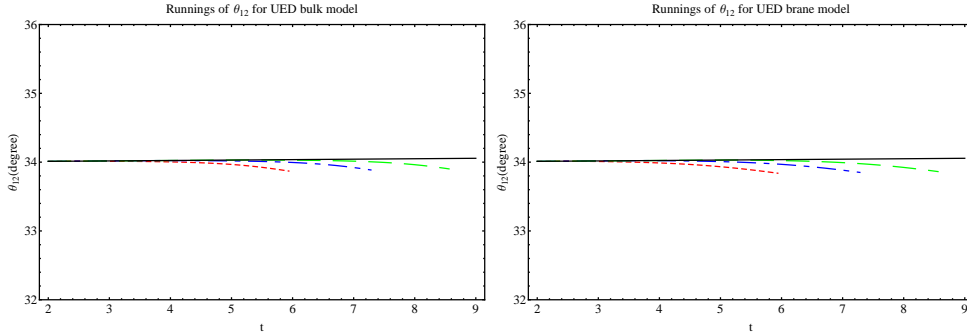


Fig. 20. Evolution of  $\theta_{12}$  as a function of the parameter  $t = \ln(\mu/M_Z)$  with matter fields in the bulk (left panel) and on the brane (right panel) respectively in the UED SM. The black line is the SM evolution, the red (small dashes) is for  $R^{-1} \sim 1$  TeV, the blue (dash-dotted)  $R^{-1} \sim 4$  TeV, and the green (large dashes)  $R^{-1} \sim 15$  TeV.



$\theta_{13} = 0$  at a high energy scale, even though the power law enhanced evolution is considered during the running. Therefore, for the tri-bimaximal mixing pattern [49], in the current context with no other extreme conditions being taken into account, a slightly changed  $\theta_{13}$  could not be accommodated during the whole range of the energy scale. Similar trajectories are also observed for  $\theta_{23}$  (see Fig. 23).

#### 9.4. $\delta$ phase

The running of the Dirac phase  $\delta$  in the UED SM case is represented in Fig.24. The variation is stable and similar for the bulk case (left panel) and brane case (right panel), there is very small deviation from the SM because all other mixing angles vary only by small quantities and the coefficient  $C$  which appear in the variation of

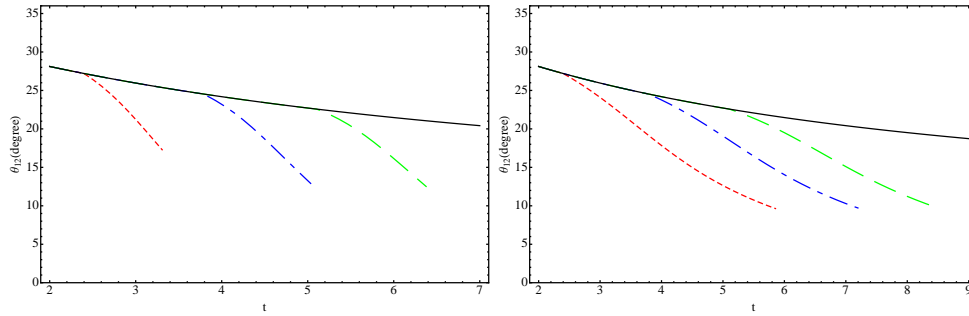


Fig. 21. Evolution of  $\theta_{12}$  in the bulk (left panel) and on the brane (right panel) as a function of the scale  $t = \ln(\mu/M_Z)$  for  $\tan\beta = 30$  in the 5D MSSM. The black line is the MSSM evolution, the red one (small dashes) is for  $R^{-1} \sim 1$  TeV, the blue (dash-dotted)  $R^{-1} \sim 4$  TeV, and the green (large dashes)  $R^{-1} \sim 15$  TeV.

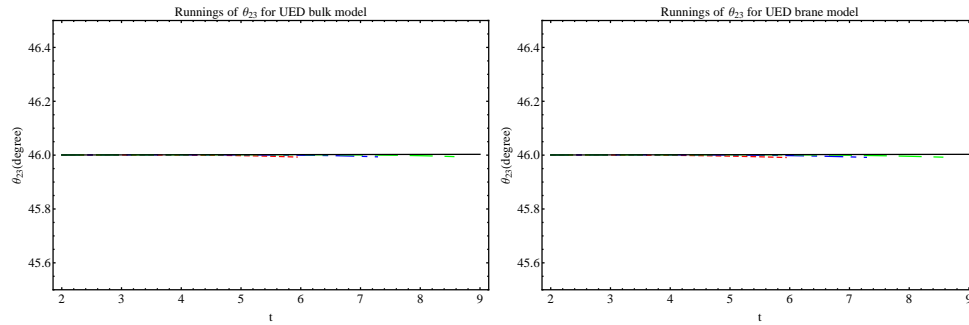


Fig. 22. Evolution of  $\theta_{23}$  as a function of the parameter  $t = \ln(\mu/M_Z)$  with matter fields in the bulk (left panel) and on the brane (right panel) respectively in the UED SM. The black line is the SM evolution, the red (small dashes) is for  $R^{-1} \sim 1$  TeV, the blue (dash-dotted)  $R^{-1} \sim 4$  TeV, and the green (large dashes)  $R^{-1} \sim 15$  TeV.

$\delta$  (see Appendix D of [24]) are linear in  $S(t)$  and there is no dependence on  $\tan\beta$ .

Noting that the Dirac phase  $\delta$  determines the strength of CP violation in neutrino oscillations. In the 5D MSSM, the runnings we include follow the general features presented in Figs.25 and 26, with large increases possible once the first KK threshold is crossed. From these studies we have seen that the variation is bigger for high  $\tan\beta$  with large changes appearing in the brane case when approaching the high energy scale. The recent results from the Daya bay and RENO reactor experiments have established a non zero values of  $\theta_{13}$ . Therefore, the leptonic CP violation characterised by the Jarlskog invariant  $J \sim \sin\theta_{12} \cos\theta_{12} \sin\theta_{23} \cos\theta_{23} \sin\theta_{13} \cos^2\theta_{13} \sin\delta$  becomes promising to be measured in the future long baseline neutrino oscillation experiments. As plotted, we can observe

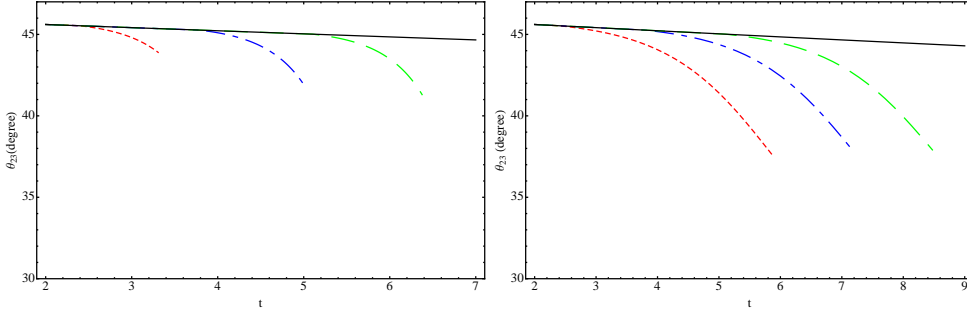


Fig. 23. Evolution of  $\theta_{23}$  in the bulk (left panel) and on the brane (right panel) as a function of the parameter  $t = \ln(\mu/M_Z)$  for  $\tan\beta = 30$  in the 5D MSSM. The black line is the MSSM evolution, the red one (small dashes) is for  $R^{-1} \sim 1$  TeV, the blue (dash-dotted)  $R^{-1} \sim 4$  TeV, and the green (large dashes)  $R^{-1} \sim 15$  TeV.

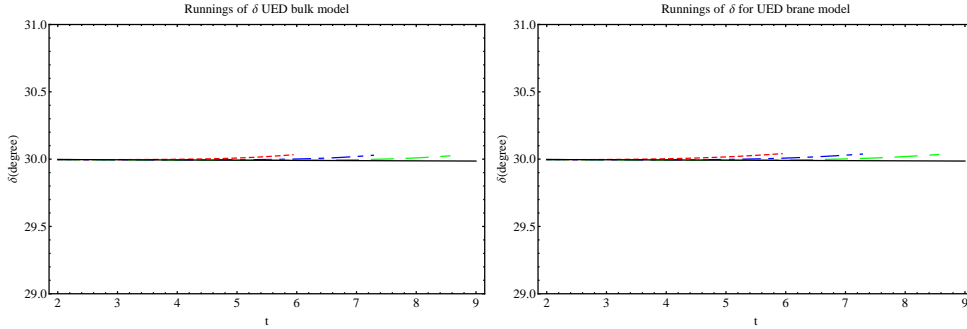


Fig. 24. Evolution of  $\delta$  as a function of the parameter  $t = \ln(\mu/M_Z)$  with matter fields in the bulk (left panel) and on the brane (right panel) respectively in the UED SM. The black line is the SM evolution, the red (small dashes) is for  $R^{-1} \sim 1$  TeV, the blue (dash-dotted)  $R^{-1} \sim 4$  TeV, and the green (large dashes)  $R^{-1} \sim 15$  TeV.

a relatively large evolution for the Dirac phase, even the maximum CP violation case  $\delta = \frac{\pi}{2}$  could be achieved for relatively small input values. For leptogenesis related to the matter-antimatter asymmetry, we should note that the parameters entering the leptogenesis mechanism cannot be completely expressed in terms of low-energy neutrino mass parameters. Note that in some specific models the parameters of the PMNS matrix (which contains CP asymmetry effects) can be used [50,51]. Here, the CP-violating effects induced by the renormalisation group corrections could lead to values of the CP asymmetries large enough for a successful leptogenesis, and the models predicting maximum leptonic CP violation, or where the CP-violating phase  $\delta$  is not strongly suppressed, become especially appealing. Specific models with large extra dimensions in which leptogenesis is relevant at low scale can also be found in

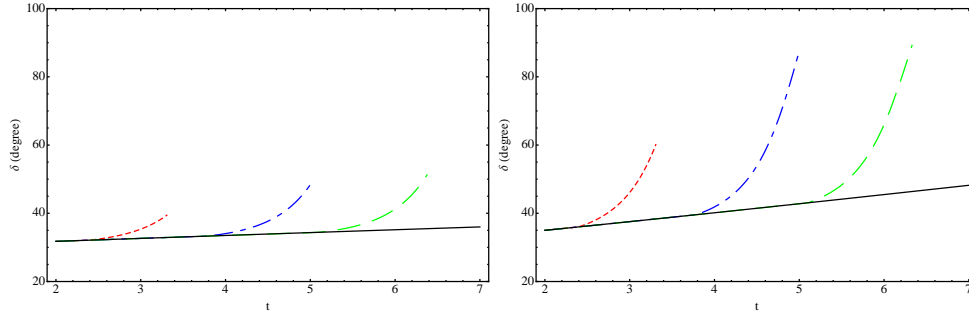


Fig. 25. Evolution of the phase  $\delta$  as a function of the parameter  $t = \ln(\mu/M_Z)$  with matter fields in the bulk for  $\tan \beta = 30$  ( left panel) and  $\tan \beta = 50$  (right panel) in the 5D MSSM respectively. The black line is the MSSM evolution, the red one (small dashes) is for  $R^{-1} \sim 1$  TeV, the blue (dash-dotted)  $R^{-1} \sim 4$  TeV, and the green (large dashes)  $R^{-1} \sim 15$  TeV.

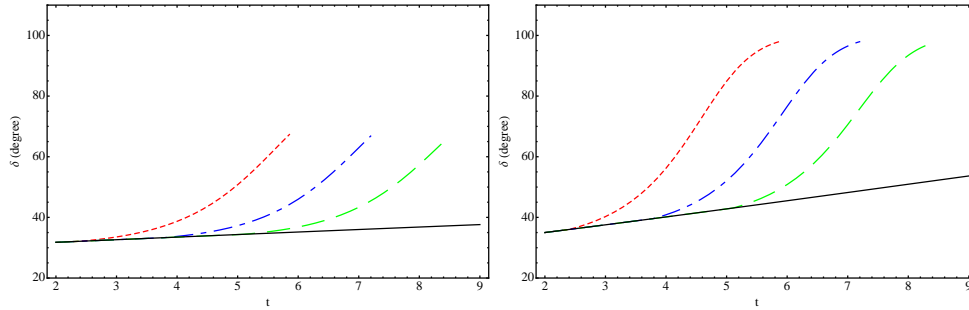


Fig. 26. Evolution of the phase  $\delta$  as a function of the parameter  $t = \ln(\mu/M_Z)$  with matter fields constrained to the brane for  $\tan \beta = 30$  ( left panel) and  $\tan \beta = 50$  (right panel) in the 5D MSSM respectively. The black line is the MSSM evolution, the red one (small dashes) is for  $R^{-1} \sim 1$  TeV, the blue (dash-dotted)  $R^{-1} \sim 4$  TeV, and the green (large dashes)  $R^{-1} \sim 15$  TeV.

Ref. [52].

The running of the mixing angles are entangled with the CP-violating phases [24]. The phases  $\phi_1$  and  $\phi_2$  do not affect directly the running of the masses, while the phase  $\delta$  has a direct effect on the size of  $dm/dt$ , although its importance is somewhat reduced by the magnitude of  $\theta_{13}$ . For further discussions of the correlation between these phases and mixing angles, refer to Refs [45, 53]. for details.

Finally, whilst the above results and analysis were for the normal hierarchy of neutrino masses, we did also consider an inverted hierarchy, where from an analysis of the equations presented in the Appendices of [24] we obtain the same features and results for neutrino mass runnings (though with different initial values at the  $M_Z$  scale). As such, the figures for  $\Delta m_{sol}^2$  and  $\Delta m_{atm}^2$  remain unchanged. Possible changes in the angles and phases arise from the different signs for the  $(m_j - m_i)/(m_j + m_i)$  terms present in each evolution equation, where the  $\theta_{12}$  results remain approximately the same (given the relative ordering of masses in these two hierarchies), and the small runnings of  $\theta_{13}$  and  $\theta_{23}$  would be up rather than down (though as already discussed, these runnings are quite small).

## 10. Summary and Outlook

The present review of the renormalisation group evolution of the masses, mixing angles and phases of the UED models in the quark and lepton sectors brings together the results we and other groups have obtained in the recent years in this subject using a common notation. The important physical points are discussed and the equations are written in compact way to show the unified approach to the different sectors of these models. For more technical details we refer to the existing literature.

Concerning the UED standard model the evolution of the gauge couplings has a rapid variation in the presence of the KK modes and this leads to a much lower unification scale than in the SM. Due to the power law running of the Yukawa couplings, the rapid decrease of the Yukawa couplings with energy is in contrast to the logarithmic running predicted by the SM. The UED model has substantial effects on the hierarchy between the quark and lepton sectors and provides a very desirable scenario for grand unification. As for the energy scaling of the Jarlskog parameter  $J$ , the contribution of KK modes is substantial. Its numerical analysis shows that its variation can be raised to more than 30%. The scale deviation of renormalisation curves from the usual SM one depends closely on the value of the compactified radius  $R$ . The smaller the radius is, the higher the energy scale we need to differentiate the UED curve from the SM one. A comparison between theoretical predictions and experimental measurements will be available once the LHC will be running at its full centre of mass energy. This will set limits on the parameters of the UED model, and a precise determination of  $J$ ,  $|V_{ub}|$  or  $|V_{cb}|$  at high energy may lead to a discrimination between the SM and extra dimensional models.

In the case of the 5D MSSM, we have reviewed the behaviour of the evolution equations for the quark and neutrino sector in a minimal supersymmetric model

with one extra-dimension. For quarks, the 5D MSSM scenarios with matter fields in the bulk or on the brane, give both results with small or no quark flavor mixings at high energies, especially for the mixings with the heavy generation. The evolution equations are particularly important in view of testing the evolution of the Yukawa couplings. The evolution of these CKM parameters have a rapid variation prior to reaching a cut-off scale where the top Yukawa coupling develops a singularity point and the model breaks down. For the brane localised matter fields model, we can only observe similar behaviour for small values of  $\tan\beta$ , while for large  $\tan\beta$ , the initial top Yukawa coupling becomes smaller, the gauge couplings then play a dominant role during the evolution of the Yukawa couplings, and therefore the Yukawa couplings decrease instead of increasing. As such the variations of these CKM parameters have a relatively milder behaviour, and the theory is valid up to the gauge coupling unification scale. Concerning the neutrino sector, the evolution equations for the mixing angles, phases,  $\Delta m_{sol}^2$  and  $\Delta m_{atm}^2$ , within the two distinct scenarios, is also considered. A larger  $\tan\beta$  typically leads to larger renormalisation group corrections. Neutrino masses evolve differently in the two models due to the sign of the (different) dominant contributions in the bulk and in the brane cases. For the brane case we find the approximate degenerate neutrino mass spectrum becomes more favourable at the ultraviolet cut-off. In the bulk case, the neutrino splitting becomes even more severe as the unitarity bounds of the effective theory are reached faster. Contrary to the large renormalisation effect of  $\theta_{12}$ , the runnings of  $\theta_{13}$  and  $\theta_{23}$  are relatively mild. We found a non-zero value for  $\theta_{13}$  during the evolution, which has no appreciable RGE running effects, even when power law evolution effects are considered. Therefore it is necessary to introduce new physics effects in order to achieve the tri-bimaximal pattern. The maximum CP violation case,  $\delta = \frac{\pi}{2}$ , could be achieved starting from a relatively small initial value. In general we can see that radiative effects may have a significant impact on neutrino physics. A non-zero Jarlskog invariant, which measures the magnitude of leptonic CP violation (expected to be measured in future long baseline neutrino oscillation experiments), could open the door for measurable CP violation in the leptonic sector.

### Acknowledgements

ASC would like to thank AD, AT and the IPNL for their hospitality during his stay in Lyon, where the first stage of this work was performed.

### Appendix A.

In the SM, the Higgs boson mass is given by  $m_H = \sqrt{\lambda}v$ , where  $\lambda$  is the Higgs self-coupling parameter and  $v$  is the vacuum expectation value of the Higgs field (where  $v = (\sqrt{2}G_F)^{-1/2} = 246$  GeV is fixed by the Fermi coupling  $G_F$ ). From the requirement that the scalar potential energy of the vacuum be bounded from below, the quartic coupling  $\lambda$  should be positive at any energy scale. If  $m_H$  is too

small,  $\lambda$  becomes negative at certain energy scales and then induces a false and deep minimum at large field values, destabilising the EW vacuum. Therefore, above that scale, the validity of the SM is expected to fail and must be embedded in some more general theories that give rise to a wealth of new physics phenomena.

In the five dimensional UED model compactified on a circle of radius  $R$  with a  $Z_2$  orbifolding, motivated by the new bounds on the mass of the SM Higgs boson around 125 GeV of ATLAS and CMS collaborations [54], we quantitatively analyse the Higgs self coupling evolution from the EW scale up to the unification scale and exploit its evolution behaviours for different compactification radii.

The kinetic term of the scalar doublet has the following forms in the 5D UED model:

$$\mathcal{L}_{Higgs} = \int_0^{\pi R} dy (D_M \Phi(x, y))^\dagger D^M \Phi(x, y), \quad (\text{A.1})$$

where the covariant derivative is

$$D_M \Phi(x, y) = \left\{ \partial_M + i g_2^5 T^a W_M + \frac{i}{2} g_1^5 B_M \right\} \Phi(x, y), \quad (\text{A.2})$$

where the gauge fields  $G_M(x, y)$   $\left(G_M^A \frac{\lambda^A}{2}\right)$ ,  $W_M(x, y)$   $\left(W_M^a \frac{\tau^a}{2}\right)$  and  $B_M(x, y)$  refer to the  $SU(3)$ ,  $SU(2)$  and  $U(1)$  gauge groups respectively. Note also the five dimensional gauge coupling constants  $g_3^5$ ,  $g_2^5$  and  $g_1^5$  are related to the four dimensional SM coupling constants (up to a normalisation factor) by  $g_i = \frac{g_i^5}{\sqrt{\pi R}}$ , and similarly for the quartic coupling  $\lambda = \frac{\lambda^5}{\sqrt{\pi R}}$ .

The evolution of the Higgs quartic coupling is given by the beta function as follows

$$16\pi^2 \frac{d\lambda}{dt} = \beta_\lambda^{SM} + \beta_\lambda^{UED}, \quad (\text{A.3})$$

where [55]

$$\begin{aligned} \beta_\lambda^{SM} = & 12\lambda^2 - \left(\frac{9}{5}g_1^2 + 9g_2^2\right)\lambda + \frac{9}{4}\left(\frac{3}{25}g_1^4 + \frac{2}{5}g_1^2g_2^2 + g_2^4\right) + 4\lambda T_t \\ & - 4Tr[3(Y_U^\dagger Y_U)^2 + 3(Y_D^\dagger Y_D)^2 + (Y_E^\dagger Y_E)^2] \end{aligned} \quad (\text{A.4})$$

where  $T_t = Tr[3Y_U^\dagger Y_U + 3Y_D^\dagger Y_D + Y_E^\dagger Y_E]$  and

$$\begin{aligned} \beta_\lambda^{UED} = & (S(t) - 1) \left\{ 12\lambda^2 - 3\left(\frac{3}{5}g_1^2 + 3g_2^2\right)\lambda + \left(\frac{9}{25}g_1^4 + \frac{6}{5}g_1^2g_2^2 + 3g_2^4\right) \right\} \\ & + 2(S(t) - 1) \left\{ 4\lambda T_t - 4Tr[3(Y_U^\dagger Y_U)^2 + 3(Y_D^\dagger Y_D)^2 + (Y_E^\dagger Y_E)^2] \right\} \end{aligned} \quad (\text{A.5})$$

for the UED bulk model, [10, 56] where both the fermion fields and the boson fields can propagate in the bulk, and

$$\beta_\lambda^{UED} = (S(t) - 1) \left\{ 12\lambda^2 - 3\left(\frac{3}{5}g_1^2 + 3g_2^2\right)\lambda + \left(\frac{9}{25}g_1^4 + \frac{6}{5}g_1^2g_2^2 + 3g_2^4\right) \right\} \quad (\text{A.6})$$

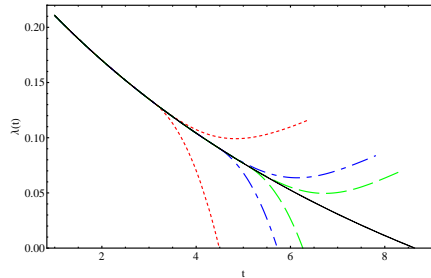


Fig. 27. The evolution of the Higgs self coupling for  $m_H = 125$  GeV, where the solid (black) line is the SM, the upward [downward] dotted (red) line is the  $R^{-1} = 2$  TeV UED brane model [UED bulk model], the upward [downward] dotted-dashed (blue) line is the  $R^{-1} = 8$  TeV UED brane model [UED bulk model], and the upward [downward] dashed (green) line is the  $R^{-1} = 15$  TeV UED brane model [UED bulk model]. The ultraviolet cutoff incurred from the vacuum instability are observed around  $t = 4.5, 5.7, 6.3$  for  $R^{-1} = 2, 8, 15$  TeV respectively in the UED bulk model.

for the UED brane model, [33] where the SM matter fields are localised to the brane, whilst the gauge and Higgs fields are propagating in the bulk. Note that the pure gauge terms in Eq. (A.6) are different from these in Ref. [43, 57]. Explicitly, these terms cannot exactly resemble what is in the SM, since there are extra contributions from the couplings of the Higgs field with the  $A_5$  component in the bulk space as well.

In Fig.27, starting from the initial value of  $m_H = 125$  GeV, we focus on the evolution of the Higgs self-coupling and explore its behaviour and constraints on the compactification radii for which the validity of the theory is satisfied. For interesting values of a Higgs mass around 125 GeV, we can observe that, in the whole range from the EW scale up to the gauge unification scale, in the UED brane model the Higgs self coupling  $\lambda(t)$  remains positive and its trajectory goes upward but remains finite when approaching the unification scale, whilst for the SM and the UED bulk model  $\lambda(t)$  evolves towards a zero value before reaching the unification scale, which then incurs the vacuum instability and introduces an ultraviolet cutoff for the theory.

## References

1. J. C. Pati and A. Salam, Phys. Rev. D **10**, 275 (1974) [Erratum-ibid. D **11**, 703 (1975)]; H. Georgi and S. L. Glashow, Phys. Rev. Lett. **32**, 438 (1974); H. Fritzsch and P. Minkowski, Annals Phys. **93**, 193 (1975); F. Gursey, P. Ramond and P. Sikivie, Phys. Lett. B **60**, 177 (1976).
2. H. Georgi, H. R. Quinn and S. Weinberg, Phys. Rev. Lett. **33**, 451 (1974).
3. K. R. Dienes, E. Dudas and T. Gherghetta, Nucl. Phys. B **537** (1999) 47 [arXiv:hep-ph/9806292]. K. R. Dienes, E. Dudas and T. Gherghetta, Phys. Lett. B **436** (1998) 55 [arXiv:hep-ph/9803466].
4. I. Antoniadis, Phys. Lett. B **246**, 377 (1990).
5. N. Arkani-Hamed and M. Schmaltz, Phys. Rev. D **61**, 033005 (2000) [hep-ph/9903417].
6. G. Servant and T. M. P. Tait, Nucl. Phys. B **650**, 391 (2003) [hep-ph/0206071].

7. T. Appelquist, H. C. Cheng and B. A. Dobrescu, Phys. Rev. D **64**, 035002 (2001) [arXiv:hep-ph/0012100].
8. N. Arkani-Hamed, H. C. Cheng, B. A. Dobrescu and L. J. Hall, Phys. Rev. D **62**, 096006 (2000) [arXiv:hep-ph/0006238].
9. T. Appelquist, B. A. Dobrescu, E. Ponton and H. U. Yee, Phys. Rev. Lett. **87**, 181802 (2001).
10. G. Bhattacharyya, A. Datta, S. K. Majee and A. Raychaudhuri, arXiv:hep-ph/0608208.
11. A. J. Buras, A. Poschenrieder, M. Spranger and A. Weiler, Nucl. Phys. B **678**, 455 (2004) [arXiv:hep-ph/0306158];  
A. J. Buras, M. Spranger and A. Weiler, Nucl. Phys. B **660**, 225 (2003) [arXiv:hep-ph/0212143].
12. D. Hooper and S. Profumo, Phys. Rept. **453**, 29 (2007) [arXiv:hep-ph/0701197];  
P. Colangelo, F. De Fazio, R. Ferrandes and T. N. Pham, Phys. Rev. D **77**, 055019 (2008) [arXiv:0709.2817 [hep-ph]] and references therein.
13. A. Datta, K. Kong and K. T. Matchev, New J. Phys. **12**, 075017 (2010) [arXiv:1002.4624 [hep-ph]].
14. M. Kobayashi and T. Maskawa, Prog. Theor. Phys. **49**, 652 (1973); N. Cabibbo, Phys. Rev. Lett. **10**, 531 (1963).
15. A. S. Cornell and L. -X. Liu, Phys. Rev. D **83** (2011) 033005 [arXiv:1010.5522 [hep-ph]].
16. L. -X. Liu and A. S. Cornell, PoS KRUGER **2010**, 045 (2010) [arXiv:1103.1527 [hep-ph]].
17. T. P. Cheng, E. Eichten and L. F. Li, Phys. Rev. D **9**, 2259 (1974).
18. A. Deandrea, J. Welzel, P. Hosteins and M. Oertel, Phys. Rev. D **75** (2007) 113005 [hep-ph/0611172].
19. C. Bouchart, A. Knochel and G. Moreau, Phys. Rev. D **84**, 015016 (2011) [arXiv:1101.0634 [hep-ph]].
20. T. Flacke, DESY-THESIS-2003-047.
21. A. Hebecker, Nucl. Phys. B **632** (2002) 101 [hep-ph/0112230].
22. N. Arkani-Hamed, T. Gregoire and J. G. Wacker, JHEP **0203**, 055 (2002) [arXiv:hep-th/0101233]. N. Marcus, A. Sagnotti and W. Siegel, Nucl. Phys. B **224**, 159 (1983). E. A. Mirabelli and M. E. Peskin, Phys. Rev. D **58**, 065002 (1998) [arXiv:hep-th/9712214]. I. L. Buchbinder, S. J. J. Gates, H. S. J. Goh, W. D. I. Linch, M. A. Luty, S. P. Ng and J. Phillips, Phys. Rev. D **70**, 025008 (2004) [arXiv:hep-th/0305169].
23. A. S. Cornell, A. Deandrea, L. -X. Liu and A. Tarhini, Phys. Rev. D **85** (2012) 056001 [arXiv:1110.1942 [hep-ph]].
24. A. S. Cornell, A. Deandrea, L. -X. Liu and A. Tarhini, arXiv:1206.5988 [hep-ph].
25. I. Antoniadis, Phys. Lett. B **246** (1990) 377; C. Csaki, arXiv:hep-ph/0404096.  
Y. A. Kubyshin, arXiv:hep-ph/0111027. V. A. Rubakov, Phys. Usp. **44**, 871 (2001) [Usp. Fiz. Nauk **171**, 913 (2001)] [arXiv:hep-ph/0104152]. A. Perez-Lorenzana, J. Phys. Conf. Ser. **18**, 224 (2005) [arXiv:hep-ph/0503177]. M. Quiros, arXiv:hep-ph/0302189;
26. N. Arkani-Hamed, T. Gregoire and J. G. Wacker, JHEP **0203** (2002) 055 [hep-th/0101233].
27. P. C. West, "Introduction to supersymmetry and supergravity,"
28. J. Wess and J. Bagger, "Supersymmetry and supergravity,"
29. J. Iliopoulos and B. Zumino, Nucl. Phys. B **76** (1974) 310; J. Wess and B. Zumino, Phys. Lett. B **49** (1974) 52.



30. P. H. Chankowski and Z. Pluciennik, Phys. Lett. B **316** (1993) 312 [hep-ph/9306333].
31. S. Antusch, M. Drees, J. Kersten, M. Lindner and M. Ratz, Phys. Lett. B **519** (2001) 238 [hep-ph/0108005].
32. K. S. Babu, Z. Phys. C **35**, 69 (1987).
33. L. -X. Liu and A. S. Cornell, arXiv:1204.0532 [hep-ph].
34. M. Bando, T. Kobayashi, T. Noguchi and K. Yoshioka, Phys. Rev. D **63**, 113017 (2001) [arXiv:hep-ph/0008120]. M. Bando, T. Kobayashi, T. Noguchi and K. Yoshioka, Phys. Lett. B **480**, 187 (2000) [arXiv:hep-ph/0002102].
35. K. Sasaki, Z. Phys. C **32**, 149 (1986).
36. M. E. Machacek and M. T. Vaughn, Nucl. Phys. B **236**, 221 (1984).
37. L. X. Liu, Int. J. Mod. Phys. A **25**, 4975 (2010), arXiv:0910.1326 [hep-ph].
38. C. Balzereit, T. Mannel and B. Plumper, Eur. Phys. J. C **9**, 197 (1999) [arXiv:hep-ph/9810350].
39. T. K. Kuo and L. X. Liu, arXiv:hep-ph/0511037.
40. Z. -z. Xing, H. Zhang and S. Zhou, Phys. Rev. D **77**, 113016 (2008) [arXiv:0712.1419 [hep-ph]].
41. K. Nakamura *et al.* [Particle Data Group Collaboration], J. Phys. G **37** (2010) 075021 and 2011 partial update for the 2012 edition.
42. S. Weinberg, Phys. Rev. Lett. **43** (1979) 1566.
43. M. Blennow, H. Melbeus, T. Ohlsson and H. Zhang, JHEP **1104** (2011) 052 [arXiv:1101.2585 [hep-ph]].
44. P. H. Chankowski and Z. Pluciennik, Phys. Lett. B **316** (1993) 312 [hep-ph/9306333]. K. S. Babu, C. N. Leung and J. T. Pantaleone, Phys. Lett. B **319** (1993) 191 [hep-ph/9309223].
45. S. Antusch, J. Kersten, M. Lindner and M. Ratz, Nucl. Phys. B **674** (2003) 401 [hep-ph/0305273].
46. M. Blennow, H. Melbeus, T. Ohlsson and H. Zhang, Phys. Lett. B **712**, 419 (2012) [arXiv:1112.5339 [hep-ph]].
47. Z. Maki, M. Nakagawa and S. Sakata, Prog. Theor. Phys. **28** (1962) 870.
48. F. P. An *et al.* [DAYA-BAY Collaboration], Phys. Rev. Lett. **108** (2012) 171803 [arXiv:1203.1669 [hep-ex]].
49. P. F. Harrison, D. H. Perkins and W. G. Scott, Phys. Lett. B **530**, 167 (2002) [hep-ph/0202074].
50. M. Raidal, A. van der Schaaf, I. Bigi, M. L. Mangano, Y. K. Semertzidis, S. Abel, S. Albino and S. Antusch *et al.*, Eur. Phys. J. C **57** (2008) 13 [arXiv:0801.1826 [hep-ph]].
51. W. Buchmuller, P. Di Bari and M. Plumacher, Nucl. Phys. B **665** (2003) 445 [hep-ph/0302092].
52. P. -H. Gu, Phys. Rev. D **81** (2010) 073002 [arXiv:1001.1340 [hep-ph]].
53. S. Luo and Z. -z. Xing, arXiv:1203.3118 [hep-ph].
54. G. Aad *et al.* [ATLAS Collaboration], Phys. Lett. B **710**, 49 (2012) [arXiv:1202.1408 [hep-ex]].  
S. Chatrchyan *et al.* [CMS Collaboration], Phys. Lett. B **710**, 26 (2012) [arXiv:1202.1488 [hep-ex]].
55. P. Kielanowski and S. R. Juarez Wysozka, Phys. Rev. D **72**, 096003 (2005).
56. A. S. Cornell and L. -X. Liu, Phys. Rev. D **84**, 036002 (2011) [arXiv:1105.1132 [hep-ph]].
57. G. Bhattacharyya, S. Goswami and A. Raychaudhuri, Phys. Rev. D **66**, 033008 (2002) [hep-ph/0202147].